CEBAF
The Continuous Electron Beam Accelerator Facility
Theory Group Preprint Series

Additional copies are available from the authors.

The Southeastern Universities Research Association (SURA) operates the Continuous Electron Beam Accelerator Facility for the United States Department of Energy under contract DE-AC05-84ER40150

DISCLAIMER

This report was prepared as an account of work sponsored by the United States government. Neither the United States nor the United States Department of Energy, nor any of their employees, makes any warranty, express or implied, or assumes any legal liability or responsibility for the accuracy, completeness, or usefulness of any information, apparatus, product, or process disclosed, or represents that its use would not infringe privately owned rights. Reference herein to any specific commercial product, process, or service by trade name, mark, manufacturer, or otherwise, does not necessarily constitute or imply its endorsement, recommendation, or favoring by the United States government or any agency thereof. The views and opinions of authors expressed herein do not necessarily state or reflect those of the United States government or any agency thereof.

CEBAF
0205 9100 003 367 0

CEBAF-TH-91-22

Nucleon Compton scattering in the nonrelativistic quark model

Simon Capstick

Department of Physics, Carnegie Mellon University, Pittsburgh, PA 15213

and Continuous Electron Beam Accelerator Facility, Newport News, VA 23606 *

B D Keister

Department of Physics, Carnegie Mellon University, Pittsburgh, PA 15213

The amplitude for Compton scattering from the nucleon is calculated within the framework of the nonrelativistic quark model. The objective is to evaluate the consistency of the model with low-energy theorems, its ability to predict the electric and magnetic polarizabilities, as well as its behavior at higher energies, where multiple nucleon resonances play a role.

I. INTRODUCTION

The electromagnetic properties of hadrons provide nontrivial constraints on attempts to model them with constituents. Compton scattering serves as an important complement to electron scattering. Within a simple nonrelativistic picture, electron scattering probes size aspects of a hadron, while Compton scattering probes its spectrum. Of course, size and spectrum are related in any model, but the ultimate test is the set of observables available from these two processes.

Compton scattering from the nucleon is constrained at very low energies by Low's theorem [1, 2], which completely fixes the contributions of $O(1)$ and $O(\omega)$ in the expansion of the scattering amplitude in powers of the photon frequency. The first structure-dependent terms come from Rayleigh scattering at $O(\omega^2)$. The coefficients $\bar{\alpha}$ and $\bar{\beta}$ are the electric and magnetic polarizabilities, respectively, and can be thought of as the Compton analog to the charge radius. At higher photon energies, the incident photon can excite a variety of intermediate nucleon resonances, and the corresponding amplitude is more sensitive to the spectral details of the model.

There has been considerable theoretical interest in computing the polarizabilities within various models, including the bag model [3, 4], the nonrelativistic quark model [5], a chiral quark model [6], the Skyrme model [7], and with chiral perturbation theory [8]. We also note that L'vov [9] obtains good agreement with available data up to 400 MeV using fixed-t dispersion relations, together with the electric and magnetic polarizabilities, as input. There are also some excellent reviews [10, 11].

Data at higher energies exists mainly in the form of differential cross-sections. These have been calculated in the $\Delta(1232)$ region and above using dispersion theory and the pion-photoproduction data [12]; this is successful in fitting the data only at low energy and for forward scattering. The Bonn group has also attempted to fit the small angle intermediate energy data using the vector (ρ) dominance model [13–16]; the $\gamma\rho$ coupling constant that results is smaller by a factor of two than the generally accepted value. Phenomenological isobar models, along with the measured photoproduction amplitudes, have been applied by the Tokyo group [17–20] to extract resonance parameters from the Compton scattering differential cross-section data.

Our goal in this study is to evaluate the performance of the nonrelativistic quark model in predicting the Compton scattering amplitude over a range of energies. To our knowledge, no calculation using a composite model for the structure of the intermediate resonances has been applied to Compton scattering at both low and intermediate energies. We believe that any quark model should attempt to be consistent with low-energy theorems, the measured polarizabilities and higher energy observables. This is a nontrivial standard. Even the low-energy theorems are not automatically satisfied within models in which Hilbert spaces are truncated or other approximations are made. We also believe that it is important to understand the role played by various ingredients of the quark model in building the Compton amplitude. These include the quality of fit to the baryon spectrum and the photon transition amplitudes, but also the possibility that baryon resonances which couple weakly to πN may figure more noticeably into a photon process.

The paper is organized as follows. In Section 2, we present basic formulas for Compton scattering, along with the salient features of the nonrelativistic quark model as they pertain to Compton scattering. We also discuss our method of calculating electromagnetic current matrix elements. The constraints provided by low-energy theorems are then given, and we show how they can be satisfied exactly for one limiting case of the model. In Section 3, we present numerical results for low-energy limits, polarizabilities, and a variety of observables at higher energies. Section 4 contains our conclusions.

II. DESCRIPTION OF THE CALCULATION

A. basic formulas for Compton scattering

We take $\hbar = c = 1$ and use Heaviside-Lorentz units, whereby $\alpha_{\rm QED} = e^2/4\pi \approx 1/137$. The Hamiltonian density for the interaction of photons with quark fields is

$$\mathcal{H}(x) = \sum_i e_i I_{i\mu}(x) A^\mu(x), \tag{1}$$

where e_i is the charge of the ith quark, $I_i^\mu(x) = \bar{q}_i(x)\gamma^\mu q_i(x)$ is the quark current, and $A^\mu(x)$ is the photon field. In a nonrelativistic valence quark model, the effective Hamiltonian has both one-photon and two-photon terms:

$$H_{\rm photon} = H_\gamma + H_{\gamma\gamma}. \tag{2}$$

The one-photon contribution is, for real transverse photons:

$$\begin{aligned} H_\gamma &= -\sum_i e_i \mathbf{I}_i(\mathbf{r}_i)\cdot\mathbf{A}(\mathbf{r}_i) \\ &= -\sum_i \left\{ \frac{e_i}{2m_i}\left[\mathbf{p}_i\cdot\mathbf{A}(\mathbf{r}_i) + \mathbf{A}(\mathbf{r}_i)\cdot\mathbf{p}_i\right] + \mu_i\cdot\nabla\times\mathbf{A}(\mathbf{r}_i)\right\}, \end{aligned} \tag{3}$$

where $\mu_i = e_i\sigma_i/2m_i$ is the magnetic moment of the ith quark, e_i, m_i, $\sigma_i/2$, $\mathbf{p}_i$ are its charge, (constituent) mass, spin, and momentum, and $\mathbf{A}(\mathbf{r}_i)$ is the photon field. The two-photon contact interaction is

$$H_{\gamma\gamma} = \sum_i \frac{e_i^2}{2m_i}[\mathbf{A}(\mathbf{r}_i)]^2, \tag{4}$$

The photon field has the following expansion:

$$\mathbf{A}(\mathbf{r}) = \sum_\lambda \int \frac{d^3k}{(2\pi)^3}\frac{1}{\sqrt{2\omega_k}}\left[a(\mathbf{k},\lambda)\hat{e}_{\mathbf{k},\lambda}e^{i\mathbf{k}\cdot\mathbf{r}} + a^\dagger(\mathbf{k},\lambda)\hat{e}^*_{\mathbf{k},\lambda}e^{-i\mathbf{k}\cdot\mathbf{r}}\right] \tag{5}$$

The Compton amplitude can be written schematically as follows:

$$T = \langle f|H_{\gamma\gamma}|i\rangle + \sum_n \frac{\langle f|H_\gamma|n\rangle\langle n|H_\gamma|i\rangle}{E_i + \omega - E_n} + \sum_n \frac{\langle f|H_\gamma|n\rangle\langle n|H_\gamma|i\rangle}{E_i - \omega' - E_n}, \tag{6}$$

where ω and ω' are the initial and final photon energies, E_i is the initial baryon energy and E_n is the energy of the intermediate hadronic state.

We now assume that the Hilbert space consists entirely of the set of baryons generated from a quark model. In addition, we assume no $(q\bar{q})$ excitations, *i.e.*, only valence quarks. In this regard, we mention recent work of Geiger and Isgur [21] on $(q\bar{q})$ excitations in mesons. First, they find that $(q\bar{q})$ excitations in mesons tend mostly to renormalize the overall string tension. Second, they consider processes such as $A \to BC \to D$. For those processes classifiable as OZI suppressed, in which the final meson D contains a $(q\bar{q})$ pair not found in the initial meson A, there may be amplitudes $A \to BC$ and $BC \to D$ which are large on an individual basis, but the *sum* of the combined amplitudes will, under certain conditions, vanish, provided that *all* intermediate $(q\bar{q})$ states are included in the sum. These results were obtained within a specific model, and make use of closure and spectator approximations. Nevertheless, interpreted in a qualitative sense, they suggest that, while amplitudes for the photoproduction of intermediate baryon+meson intermediate states may be individually large, there may also be considerable cancellation among them, and that it would be better to leave meson [or $(q\bar{q})$] excitations out of the calculation entirely than to include only a partial sum. In the exploratory calculation presented here, we take the former option. Pionic excitation, however, may be a special case, as is discussed in our conclusions.

If the γN system has an overall momentum $\mathbf{P}$, and the initial and final photon momenta are $\mathbf{k}$ and $\mathbf{k}'$, respectively, then the Compton amplitude is

$$T = e^2 \sum_{r,s} \frac{1}{\sqrt{2\omega'}\sqrt{2\omega}}\epsilon'_r T_{rs}\epsilon_s, \tag{7}$$

where

$$\begin{aligned} T_{rs} = &\sum_i \langle N;\mathbf{P}-\mathbf{k}'|\frac{e_i^2}{2e^2m_i}\delta_{rs}|N;\mathbf{P}-\mathbf{k}\rangle \\ &+ \sum_n \frac{\langle N;\mathbf{P}-\mathbf{k}'|I_r(0)|X_n;\mathbf{P}\rangle\langle X_n;\mathbf{P}|I_s(0)|N;\mathbf{P}-\mathbf{k}\rangle}{\omega + \omega_{M_N}(\mathbf{P}-\mathbf{k}) - \omega_{M_n}(\mathbf{P})} \\ &+ \sum_n \frac{\langle N;\mathbf{P}-\mathbf{k}'|I_r(0)|X_n;\mathbf{P}-\mathbf{k}-\mathbf{k}'\rangle\langle X_n;\mathbf{P}-\mathbf{k}-\mathbf{k}'|I_s(0)|N;\mathbf{P}-\mathbf{k}\rangle}{-\omega' + \omega_{M_N}(\mathbf{P}-\mathbf{k}) - \omega_{M_n}(\mathbf{P}-\mathbf{k}-\mathbf{k}')}, \end{aligned} \tag{8}$$

where

$$\omega_m(\mathbf{p}) := \sqrt{m^2+\mathbf{p}^2}, \tag{9}$$

and X_n stands for any baryon in the spectrum.

B. overview of the nonrelativistic quark model

The wavefunctions for the nucleon and delta resonances used here are those of the nonrelativistic quark model (NRQM), specifically the model of Isgur and Karl [22, 23], which describes a baryon as three valence quarks moving in a confining potential. The Schrödinger equation for the nonrelativistic three body system is solved for baryon energies and compositions using the Hamiltonian

$$H = \sum_i \left(m_i + \frac{\mathbf{p}_i^2}{2m_i}\right) + \sum_{i<j}\left(V^{ij} + H^{ij}_{\rm hyp}\right), \tag{10}$$

where the spin-independent potential V^{ij} has the form

$$V^{ij} = c + \frac{br_{ij}}{2} - \frac{2\alpha_s}{3r_{ij}}, \tag{11}$$

with $\mathbf{r}_{ij} = \mathbf{r}_i - \mathbf{r}_j$. The hyperfine interaction $H^{ij}_{\rm hyp}$ is the sum

$$H^{ij}_{\rm hyp} = \frac{2\alpha_s}{3m_im_j}\left\{\frac{8\pi}{3}\mathbf{S}_i\cdot\mathbf{S}_j\delta^3(\mathbf{r}_{ij}) + \frac{1}{r_{ij}^3}\left[\frac{3(\mathbf{S}_i\cdot\mathbf{r}_{ij})(\mathbf{S}_j\cdot\mathbf{r}_{ij})}{r_{ij}^2} - \mathbf{S}_i\cdot\mathbf{S}_j\right]\right\} \tag{12}$$

of familiar contact and tensor terms arising from the (color) magnetic dipole-magnetic dipole interaction. In practice, V^{ij} is written in terms of a harmonic-oscillator potential plus an anharmonicity

$$V^{ij} = \frac{Kr_{ij}^2}{2} + U_{ij}, \tag{13}$$

and the resulting anharmonic terms are treated perturbatively.

States of the three-quark system which represent the nucleons and deltas (with three equal-mass quarks) are then written as the product of a totally antisymmetric (under the exchange group S_3) color wavefunction and a totally symmetric sum

$$\Psi = C_A \sum \psi\chi\phi, \tag{14}$$

where the spatial (ψ), spin (χ), and flavor (ϕ) wavefunctions form representations of S_3. The zeroeth order spatial wavefunctions are therefore taken to be the harmonic-oscillator eigenfunctions $\psi_{NLM}(\boldsymbol{\rho}, \boldsymbol{\lambda})$ with $\boldsymbol{\rho} = (\mathbf{r}_1 - \mathbf{r}_2)/\sqrt{2}$ and $\boldsymbol{\lambda} = (\mathbf{r}_1 + \mathbf{r}_2 - 2\mathbf{r}_3)/\sqrt{6}$. Ground states [such as $N(938)$ and $\Delta(1232)$] are described (to zeroeth order) by wavefunctions with $N = 2(n_\rho + n_\lambda) + l_\rho + l_\lambda = 0$, which means they have no radial nodes or angular momentum. The negative-parity excited nucleon and delta resonances ('P waves') in the 1.5–1.7 GeV region have $N = 1$ spatial wavefunctions with either $l_\rho = 1$ or $l_\lambda = 1$, and the positive parity excited resonances in the 1.5–2.0 GeV region have $N = 2$ wavefunctions. In order to describe the intermediate states in our calculation we need to establish the notation of the Isgur-Karl model for the unmixed harmonic-oscillator states. The details of how the sums in Eq. 14 are constructed can be found in Refs. [22] and [23]; here we just use the labels for the unmixed states which result from that procedure. Individual oscillator substates are labeled $|X^{2S+1}L_\pi J^P\rangle$, where $X = N$ or Δ, S is the total quark spin, L is the orbital angular momentum, π is the S_3 symmetry of the spatial wavefunction (S=symmetric, M=mixed, and A=antisymmetric), and J^P are the total angular momentum and parity of the state. We will also find it convenient to group the states into $SU(6)$ multiplets, labeled by $[\mu, L^P]$, where μ is the SU(6) multiplicity (found from the spin and flavor multiplicity of a group of states with similar spatial wavefunctions) and L^P is the orbital angular momentum and parity of the spatial wavefunction. For example, the ground state nucleon $|N^2S_S\frac{1}{2}^+\rangle$ and delta $|\Delta^4S_S\frac{3}{2}^+\rangle$ are found in the $[56, 0^+]$ multiplet, while the $S_{11}(1535)$ P-wave resonance is a mixture of the oscillator substates $|N^2P_M\frac{1}{2}^-\rangle$ and $|N^4P_M\frac{1}{2}^-\rangle$ found in the $[70, 1^-]$ multiplet. All of the states up to the $N = 2$ band are tabulated in Table I.

The energies and compositions of the resonances are then modeled by first-order perturbation theory in the anharmonicity U_{ij} and the hyperfine interaction $H_{\rm hyp}^{ij}$. The anharmonicity is treated as a diagonal perturbation on the energies of the states; in particular it is used only to split the $N = 2$ band (it causes no

splittings to first order in the $N = 0$ or $N = 1$ bands). The diagonal expectations of U in the $N = 0$ and $N = 1$ bands are lumped into the band energies; the mixing of states between the $N = 0$ and $N = 2$ bands induced by U is ignored. The hyperfine interaction is treated to first order in both the energies and wavefunctions, with the contact interaction active within all bands and the tensor interaction active within the $N = 1$ and $N = 2$ bands. In their paper on positive parity excited baryons, Isgur and Karl [23] quoted wavefunctions for the excited $J^P = \frac{1}{2}^+$ nucleons and $J^P = \frac{3}{2}^+$ deltas which do not include the mixings with the ground states that were later calculated and shown to have important physical consequences by Isgur, Karl and Koniuk [24]. As a result, these wavefunctions are not orthogonal to the (properly) mixed ground states from Ref. [24]; this is corrected here (in our 'mixed' basis) by re-diagonalising the hyperfine (plus diagonal-anharmonic) interaction in the combined $N = 0$ and $N = 2$ basis.

The main features of the spectrum of the P-wave and positive-parity excited baryons are then quite convincingly described by this model. The effective parameter α_s sets the scale of the hyperfine interactions and can be adjusted to fit the $\Delta(1232)$–nucleon splitting. The structure of the splittings of the P-wave resonances is then determined; the contact interaction is responsible for splitting the $|N^2P_M\frac{1}{2}^-\rangle$ and $|N^2P_M\frac{3}{2}^-\rangle$ below the other states, and then the tensor interaction introduces further (smaller) splittings, and mixings of the N^4 and N^2 states. The resulting spectrum is in rough agreement with the experimental pattern, and just as importantly the compositions of the mixed $|N\frac{1}{2}^-\rangle$ and $|N\frac{3}{2}^-\rangle$ states is in agreement with details of their strong decays. The $N = 2$ band spectrum has its coarse structure determined by the splitting induced by the anharmonicity, which in first order perturbation theory is independent of the exact form of $U_{ij} = U(r_{ij})$; the size of the splittings can therefore be parametrized by a constant Δ. Choosing Δ larger than the oscillator level splitting ω can (rather artificially) force the lightest nucleon resonance in this band, the $|N^2S_{S'}\frac{1}{2}^+\rangle$ in the $[56', 0^+]$ multiplet, to be lighter than the P-wave states, and so it can be associated with the Roper resonance $N(1440)$. The anharmonicity produces splittings between the other $SU(6)$ multiplets, and the contact and tensor parts of the hyperfine interaction cause splittings and mixings of all states with the same isospin and J. There are more states predicted by the model in the $N = 2$ band than exist in the πN partial wave analysis data; a strong decay analysis carried out by Koniuk and Isgur [25] established that the states whose mixed wavefunctions allow them to couple to their πN production channel correspond, in both energy and number, with the observed states.

C. electromagnetic current matrix elements in the nonrelativistic quark model

The transverse components of the electromagnetic current operator which we use here were calculated in this basis of mixed wavefunctions by Koniuk and Isgur [25]. They used a nonrelativistic transition operator based on the interaction Hamiltonian H_γ given in Eq. 3. Their purpose was to calculate the photo-excitation amplitudes for the nucleon and delta resonances formed in $\gamma N \rightarrow X \rightarrow \pi N$ (real photons) in the center of mass frame of the excited resonance X. These two transverse amplitudes $A_{\frac{1}{2}}$ and $A_{\frac{3}{2}}$ are defined in terms of helicity states of the nucleon and the produced resonance by

$$A_\lambda = \langle XJ; \mathbf{0}\lambda | I_\lambda(0) | N\tfrac{1}{2}; -\mathbf{k}\lambda_N \rangle, \tag{15}$$

where $\lambda_N = 1-\lambda$, and the matrix element is to be evaluated in the rest frame of X with $\mathbf{k}||\hat{\mathbf{z}}$. Note that $A_{\frac{3}{2}}$ is forbidden in the case that X has $J = \frac{1}{2}$. The resulting fit of the photo-excitation amplitudes of the baryon resonances by Koniuk and Isgur [25] is of poorer quality than the spectral fit, as we might expect from the results of a perturbative treatment. We will return to this point in our discussion of the results of our calculation at higher energies.

Modern calculations [26–28] have gone beyond Isgur and Karl's model for the spectrum and wavefunctions, and beyond the nonrelativistic approximation [29, 30] for the electromagnetic transition operator; we hope to apply a more sophisticated model of this type to Compton scattering in the future.

To use the Isgur-Karl-Koniuk model in our calculation, we need all four matrix elements of the electromagnetic current. In order to describe their calculation, we examine the details of how an effective operator to be used between NRQM wavefunctions for the intermediate resonances and the nucleon is derived. If we insert the field $\mathbf{A}(\mathbf{r}_i)$ defined in Eq. 5 into Eq. 3, then we can write the transverse amplitudes as

$$\frac{e}{\sqrt{2\omega}} A_\lambda = \sum_i \langle XJ; \lambda | H_i^t | N\tfrac{1}{2}; \lambda - 1 \rangle. \tag{16}$$

Here the expectation value is taken to mean integration over $\boldsymbol{\rho}$, $\boldsymbol{\lambda}$ and $\mathbf{R} = (\mathbf{r}_1 + \mathbf{r}_2 + \mathbf{r}_3)/3$, and expectation value of spin and flavor dependent quantities between the spin wavefunctions $\chi_X^\dagger$ and χ_N, and the flavor wavefunctions $\phi_X^\dagger$ and ϕ_N.

Since the wavefunctions in Eq. 14 are explicitly symmetrized, it is sufficient to know the form of the operator for the third quark in the sum in Eq. 3. We can write H_3^t in Eq. 16 as

$$H_3^t = \frac{e_3}{m} \frac{1}{\sqrt{2}} \frac{1}{\sqrt{2\omega}} \left(p_{3+} + k \frac{\sigma_{3+}}{2} \right) e^{ikr_{3z}}, \tag{17}$$

where we have used the polarization vector $\epsilon_{+1} = \frac{-1}{\sqrt{2}}(1, i, 0)$. We then integrate over the center of mass coordinate $\mathbf{R}$ (note that $\mathbf{r}_3 = \mathbf{R} - \sqrt{\frac{2}{3}}\boldsymbol{\lambda}$) after inserting plane waves for the center of mass motion for the initial and final baryons (one with momentum zero). The result is that Eq. 16 can be written as a simple integral over internal coordinates

$$\frac{e}{\sqrt{2\omega}} A_\lambda = 3\langle XJ; \lambda | H_3^t | N\tfrac{1}{2}; \lambda - 1 \rangle. \tag{18}$$

with the operator

$$H_3^t \rightarrow -\frac{e_3}{m} \frac{1}{\sqrt{2}} \frac{1}{\sqrt{2\omega}} e^{-ik\sqrt{\frac{2}{3}}\lambda_z} \left(\sqrt{\frac{2}{3}} p_{\lambda+} - k \frac{\sigma_{3+}}{2} \right). \tag{19}$$

In a similar way we can write the longitudinal current matrix element as

$$\frac{e}{\sqrt{2\omega}} L_{\frac{1}{2}} = 3\langle XJ; \tfrac{1}{2} | H_3^l | N\tfrac{1}{2}; \tfrac{1}{2} \rangle, \tag{20}$$

with

$$H_3^l \rightarrow \frac{e_3}{m} \frac{1}{\sqrt{2\omega}} \left(\sqrt{\frac{2}{3}} p_{\lambda z} + \frac{k}{2} \right) e^{-ik\sqrt{\frac{2}{3}}\lambda_z}, \tag{21}$$

and the charge matrix element as

$$\frac{e}{\sqrt{2\omega}} C_{\frac{1}{2}} = 3\langle XJ; \tfrac{1}{2} | H_3^s | N\tfrac{1}{2}; \tfrac{1}{2} \rangle, \tag{22}$$

with

$$H_3^s \rightarrow -e_3 \frac{1}{\sqrt{2\omega}} e^{-ik\sqrt{\frac{2}{3}}\lambda_z}. \tag{23}$$

D. boosts of current matrix elements

The key physical ingredient in the calculation of Compton scattering amplitudes is the set of current matrix elements between the target nucleon and each of the excited baryons included in the spectrum. For real photons, only matrix elements of the transverse components of the currents are in principle required. However, because the current matrix elements are calculated in the rest frame of the excited baryon, the need for transverse matrix elements in the presence of the crossed-photon process also requires us to calculate *all* components of the

current in the excited baryon rest frame. Since the quark model itself is nonrelativistic, Lorentz transformations of current matrix elements cannot be done fully consistently. In the face of this, we proceed as follows. For each excited baryon, the transition current matrix elements can be expressed in any frame via Lorentz invariant form factors. These form factors are computed specifically in terms of the transition matrix elements in the excited baryon rest frame. The lack of full relativistic consistency would appear when we tried to compute the transition matrix elements in some other frame and found different "Lorentz invariant" form factors.

We use a Lorentz covariant multipole expansion to express the physical information in the transition current matrix elements. The details are summarized in Ref. [31] We provide the salient details here.

The four-vector current operator $I^\mu(x)$ can be expressed in terms of a 2×2 matrix as follows:

$$\bar{I}^\alpha_{\dot\beta}(x) = \left[i\sigma_2\{I^0(x) + \mathbf{I}(\mathbf{x})\cdot\boldsymbol{\sigma}\}\right]^\alpha_{\dot\beta}(x), \tag{24}$$

where $\boldsymbol{\sigma}$ are the Pauli matrices. Then $\bar{I}^\alpha_{\dot\beta}(x)$ transforms according to the undotted and dotted representations of $SL(2,C)$. The matrix element can be written as follows: Matrix elements of $\bar{I}^\alpha_{\dot\beta}(0)$ can then be expressed in terms of reduced matrix elements as follows:

$$\begin{aligned}
&\langle XJ_X;\mathbf{p}'\mu'|\bar{I}^\alpha_{\dot\beta}(0)|N\tfrac{1}{2};\mathbf{p}\mu\rangle \\
&\quad= \sqrt{\frac{m'}{\omega_{m'}(\mathbf{p}')}}\sqrt{\frac{\omega_m(\mathbf{p}_0)}{\omega_m(\mathbf{p})}}\sum\langle\tfrac{1}{2}\zeta\tfrac{1}{2}\dot\eta|s\mu_s\rangle\langle l\mu_l s\mu_s|\mathcal{J}\mu_{\mathcal{J}}\rangle\langle j\bar\mu\mathcal{J}\mu_{\mathcal{J}}|j'\mu'\rangle Y^{l}_{\mu_l}{}^*(\hat{\mathbf{p}}_0) \\
&\qquad\times[L_c^{-1}(p')]_{\zeta\alpha}[L_c(p')]^\dagger_{\dot\eta\dot\beta}D^{j\dagger}_{\bar\mu\mu}[R_c(L_c(p'),p_0)]\langle XJ_X\|\bar{I}_{ls\mathcal{J}}(q^2)\|N\tfrac{1}{2}\rangle.
\end{aligned} \tag{25}$$

The momentum $\mathbf{p}_0$ is the momentum of the initial nucleon in the rest frame of the excited baryon. $L_c(p)$ is a 2×2 representation of a rotationless boost under $SL(2,C)$:

$$L_c(p) := \cosh\tfrac{1}{2}u + \boldsymbol{\sigma}\cdot\hat{\mathbf{p}}\sinh\tfrac{1}{2}u; \qquad \tanh u = |\mathbf{p}|/p^0, \tag{26}$$

corresponding to the transformation of a particle at rest to a momentum p^μ. The Wigner rotation $R_c(\Lambda,p)$ corresponds to a Lorentz transformation between momentum p^μ and $p'^\mu = \Lambda^\mu{}_\nu p^\nu$:

$$R_c(\Lambda,p) := L_c^{-1}(\Lambda p)\Lambda L_c(p). \tag{27}$$

To make a connection between $\bar{I}^\alpha_{\dot\beta}(x)$ and $I^\mu(x)$, we define

$$\hat{I}^s_{\mu_s}(x) := (-1)^s\frac{1}{\sqrt{2}}\sum_{\alpha\dot\beta}\langle\tfrac{1}{2}\alpha\tfrac{1}{2}\dot\beta|s\mu_s\rangle I^\alpha_{\dot\beta}(x), \tag{28}$$

which has explicit components

$$\hat{I}^1_{\pm1}(x) = \mp\frac{1}{\sqrt{2}}(I^1(x)\pm iI^2(x)); \qquad \hat{I}^1_0(x) = I^3(x); \tag{29}$$

$$\hat{I}^0_0(x) = I^0(x). \tag{30}$$

Note that Eq. 28 is simply a definition, and does not imply that $\hat{I}^s_{\mu_s}$ has the rotational properties of a rank-s tensor. The matrix elements of $\hat{I}^s_{\mu_s}(0)$ can then be expressed as follows:

$$\begin{aligned}
&\langle XJ_X;\mathbf{p}'\mu'|\hat{I}^s_{\mu_s}(0)|N\tfrac{1}{2};\mathbf{p}\mu\rangle \\
&\quad= (-1)^s\frac{1}{\sqrt{2}}\sqrt{\frac{m'}{\omega_{m'}(\mathbf{p}')}}\sqrt{\frac{\omega_m(\mathbf{p}_0)}{\omega_m(\mathbf{p})}}\sum\langle\tfrac{1}{2}\alpha\tfrac{1}{2}\dot\beta|s\mu_s\rangle\langle\tfrac{1}{2}\zeta\tfrac{1}{2}\dot\eta|s\mu_s\rangle \\
&\qquad\times\langle l\mu_l s\mu_s|\mathcal{J}\mu_{\mathcal{J}}\rangle\langle j\bar\mu\mathcal{J}\mu_{\mathcal{J}}|j'\mu'\rangle Y^{l}_{\mu_l}{}^*(\hat{\mathbf{p}}_0) \\
&\qquad\times[L_c^{-1}(p')]_{\zeta\alpha}[L_c(p')]^\dagger_{\dot\eta\dot\beta}D^{j\dagger}_{\bar\mu\mu}[R_c(L_c(p'),p_0)]\langle XJ_X\|\bar{I}_{ls\mathcal{J}}(q^2)\|N\tfrac{1}{2}\rangle.
\end{aligned} \tag{31}$$

The reduced matrix elements $\langle XJ_X\|\bar{I}_{ls\mathcal{J}}(q^2)\|N\frac{1}{2}\rangle$ are Lorentz invariant and contain all the dynamical information relevant to any electromagnetic transition matrix elements between two states with a given mass and spin. However, these reduced matrix elements are not all independent: beyond the requirement of Poincaré covariance of the matrix elements, there are additional symmetries which further constrain them.

The constraint of current continuity can be written as

$$q^0\langle XJ_X;\mathbf{p}'\mu'|I^0(0)|N\tfrac{1}{2};\mathbf{p}\mu\rangle - \mathbf{q}\cdot\langle XJ_X;\mathbf{p}'\mu'|\mathbf{I}(0)|N\tfrac{1}{2};\mathbf{p}\mu\rangle = 0. \tag{32}$$

This equation, together with Eq. 30, means that reduced matrix elements of $\hat{I}^0_0(0)$ can always be re-expressed in terms of matrix elements of $\hat{I}^1_\mu(0)$, or equivalently, matrix elements of the three-vector current $\mathbf{I}(0)$.

The output of the nonrelativistic quark model is a set of helicity amplitudes, which are defined in terms of matrix elements of $\hat{I}^s_\mu(0)$ as follows:

$$\begin{aligned}
C_{\frac{1}{2}} &= \langle XJ_X;\mathbf{0}\tfrac{1}{2}|\hat{I}^0_0(0)|N\tfrac{1}{2};-\mathbf{k}\tfrac{1}{2}\rangle; \\
L_{\frac{1}{2}} &= \langle XJ_X;\mathbf{0}\tfrac{1}{2}|\hat{I}^1_0(0)|N\tfrac{1}{2};-\mathbf{k}\tfrac{1}{2}\rangle; \\
A_{\frac{1}{2}} &= \langle XJ_X;\mathbf{0}\tfrac{1}{2}|\hat{I}^1_1(0)|N\tfrac{1}{2};-\mathbf{k}-\tfrac{1}{2}\rangle; \\
A_{\frac{3}{2}} &= \langle XJ_X;\mathbf{0}\tfrac{1}{2}|\hat{I}^1_1(0)|N\tfrac{1}{2};-\mathbf{k}\tfrac{1}{2}\rangle,
\end{aligned} \tag{33}$$

corresponding to the Coulomb, longitudinal and the two transverse amplitudes, respectively. In the rest frame of the excited baryon, Eq. 25 has an even simpler form:

$$\langle X J_X; \mathbf{0}\mu' | \bar{I}^{\alpha}_{\beta}(0) | N\tfrac{1}{2}; \mathbf{p}_0\mu\rangle = \sum \langle \tfrac{1}{2}\alpha \tfrac{1}{2}\dot{\beta} | s\mu_s\rangle \langle l\mu_l s\mu_s | \mathcal{J}\mu_{\mathcal{J}}\rangle \langle j\mu\mathcal{J}\mu_{\mathcal{J}} | j'\mu'\rangle \times Y^{l}_{\mu_l}{}^{*}(\hat{\mathbf{p}}_0) \langle X J_X \| \bar{I}_{ls\mathcal{J}}(q^2) \| N\tfrac{1}{2}\rangle. \quad (34)$$

Of the four helicity amplitudes, only three are independent, the fourth being constrained by current conservation. There are also four corresponding reduced matrix elements $\langle X J_X \| \bar{I}_{l[\frac{1}{2}\frac{1}{2}]s\mathcal{J}}(q^2) \| N\frac{1}{2}\rangle$ which are consistent with spatial inversion symmetry, and the continuity relation reduces this number to three. Eqs. 33 and 34 can then be solved to relate the reduced matrix elements to the helicity amplitudes. For $j' = \frac{1}{2}$, there are only three helicity amplitudes and corresponding reduced matrix elements, of which only two are independent under the constraint of current continuity.

As an application of this procedure, we compute the elastic electron-scattering form factors for the proton and neutron. The Sachs form factors $G_E(Q^2)$ and $G_M(Q^2)$ are related to current matrix elements in the nucleon Breit frame as follows:

$$\langle N\tfrac{1}{2}; +\tfrac{1}{2}\mathbf{q}\mu' | I^0(0) | N\tfrac{1}{2}; -\tfrac{1}{2}\mathbf{q}\mu\rangle = \delta_{\mu'\mu} \frac{G_E(Q^2)}{\sqrt{1+\tau}};$$

$$\langle N\tfrac{1}{2}; +\tfrac{1}{2}\mathbf{q}\mu' | \mathbf{I}(0) | N\tfrac{1}{2}; -\tfrac{1}{2}\mathbf{q}\mu\rangle = i(\sigma \times \mathbf{q})_{\mu'\mu} \frac{G_M(Q^2)}{\sqrt{1+\tau}}, \quad (35)$$

where $\tau := Q^2/4M^2$ and $Q^2 = \mathbf{q}^2$ in the Breit frame. A boost of the current matrix elements is necessary because the helicity amplitudes A_λ, C_λ and L_λ are computed in the rest frame of the final nucleon rather than the Breit frame.

The form factors are plotted in Fig. 1, together with modified dipole form factors:

$$G_{Ep}(Q^2)_{\text{dipole}} = \frac{1}{1 + Q^2/\Lambda^2};$$
$$G_{Mp}(Q^2)_{\text{dipole}} = \mu_p G_{Ep}(Q^2)_{\text{dipole}};$$
$$G_{Mn}(Q^2)_{\text{dipole}} = \mu_n G_{Ep}(Q^2)_{\text{dipole}};$$
$$G_{En}(Q^2)_{\text{dipole}} = -\tau G_{Mn}(Q^2)_{\text{dipole}}. \quad (36)$$

For $\Lambda^2 = 0.71\,\text{GeV}^2$, the dipole form factor represents a reasonable fit to existing data, at least for purposes of comparison. All of the Isgur-Karl form factors fall off too slowly for low Q^2. As is well known, this means that the predicted charge

radius is too small: 0.4 fm *vs.* 0.8 fm. In addition, the form factors fall off too rapidly at large Q^2. Most likely, this is a consequence of using a truncated harmonic-oscillator basis.

E. low-energy limit

The low-energy behavior of the nucleon Compton amplitude can be characterized by an expansion of the amplitude in powers of the photon frequency. As shown by Low [1] and by Gell-Mann and Goldberger [2], the contributions of $O(1)$ and $O(\omega)$ are completely determined by the nucleon mass and magnetic moment. At $O(\omega^2)$, two new contributions enter, namely, the electric and magnetic polarisabilities. It can be shown, using methods similar to that used to prove Low's theorem [32, 33], that the *structure* of the amplitudes is completely determined, though the actual polarizabilities α and β depend upon the composite physics of the nucleon. For the nucleon in the lab frame, the complete expression is [32]

$$\begin{aligned} T = \frac{e^2}{M}\Bigg\{ & (\epsilon'\cdot\epsilon) - i(\omega'+\omega)\frac{(1+2\lambda)}{4M}\sigma\cdot(\epsilon'\times\epsilon) \\ & + i(\omega'+\omega)\frac{(1+\lambda)^2}{4M}\sigma\cdot(\mathbf{n}'\times\epsilon')\times(\mathbf{n}\times\epsilon) \\ & - i\frac{(1+\lambda)}{2M}\left[\omega'(\mathbf{n}'\cdot\epsilon)\sigma\cdot(\mathbf{n}'\times\epsilon') - \omega(\mathbf{n}'\cdot\epsilon')\sigma\cdot(\mathbf{n}\times\epsilon)\right] \\ & - \omega'\omega\frac{(2\lambda+\lambda^2)}{4M^2}(\epsilon'\cdot\epsilon) + \omega'\omega\frac{(1+\lambda)^2}{4M^2}(\mathbf{n}'\times\epsilon')\cdot(\mathbf{n}\times\epsilon)(\mathbf{n}'\cdot\mathbf{n}) \\ & - \omega'\omega\frac{1}{4M^2}(\mathbf{n}\cdot\epsilon)(\mathbf{n}'\cdot\mathbf{n}) \\ & - \omega'\omega\frac{\bar{\alpha}}{M^2}(\epsilon'\cdot\epsilon) - \omega'\omega\frac{\bar{\beta}}{M^2}(\mathbf{n}'\times\epsilon')\cdot(\mathbf{n}\times\epsilon)\Bigg\} + O(\omega^3), \end{aligned} \quad (37)$$

where λ is the anomalous nucleon magnetic moment, $\mathbf{k} = \omega\mathbf{n}$ and $\mathbf{k}' = \omega'\mathbf{n}'$.

A calculated nucleon Compton amplitude should therefore be capable of reproducing the behavior dictated by the low-energy theorems as well as correctly predicting the polarizabilities. However, reproducing the low-energy theorems is not guaranteed for any calculation: indeed, there are many ways for a calculation to fail to yield the low-energy behavior. For example, since the Thomson limit ($O(1)$) for Compton scattering from a charged particle has the contact form $(e^2/m)(\epsilon'\cdot\epsilon)$, one would be tempted to assume that the Thomson limit for a composite particle is simply the sum of the Thomson limits of the constituents. In general, however,

$$\frac{e^2}{m} \neq \sum_i \frac{e_i^2}{m_i}. \tag{38}$$

The problem is resolved when one takes into account the *non-contact* contributions (those involving matrix elements of one-photon operators as opposed to two-photon operators), while keeping track of the Fermi motion of the constituent particles and the recoil of the final composite particle in the lab. Indeed, it has been shown by explicit calculation [34, 35] that these contributions combine to yield the result dictated by the low-energy theorem.

The original proofs of Low's theorem [1, 2] were essentially model independent. Later works [34, 35] centered on classes of models, and used closure over the spectrum of the strong-interaction Hamiltonian to obtain the low-energy result. This presents a potential problem for calculations based upon a specific model which are intended to produce a Compton amplitude over a range of energies, and not just at threshold. A closure sum could only be performed at threshold; at nonzero energies a truncation of the model space is a practical requirement. Nevertheless, a calculation employing a truncated model space runs the risk of violating the low energy theorem, if the closure sum at threshold depends in an essential way upon the truncated states.

A special case which offers a partial resolution of this dilemma is the harmonic-oscillator model. Near threshold, the non-contact term is dominated by processes in which intermediate states are excited by the convection current. The corresponding gradient operator converts the lowest lying S state into a multiple of the lowest lying P-wave state. Only one state is excited, and the closure sum therefore saturates with this one state at threshold. This result has been verified explicitly for a model of a charged spin-$\frac{1}{2}$ particle bound to a spinless uncharged spectator. A direct verification at threshold for antisymmetric three-quark wave functions is technically more involved, but the result must be the same. This can be seen by noting that Low's derivation of the low-energy Thomson limit is a consequence of the continuity equation. Since the harmonic-oscillator model is a local interaction which does not transfer charge between constituent quarks, its one-body currents satisfy the continuity equation. We expect therefore that the Thomson limit will be obtained with a complete sum over the excited baryon spectrum, and in fact it will saturate with the lowest-lying P-wave states because of the particular symmetry of the harmonic-oscillator wave functions.

While reproducing the Thomson limit in a particular model is certainly feasible, as discussed above, correctly obtaining the $O(\omega)$ contribution is unlikely in a nonrelativistic calculation. Low's derivation of the $O(\omega)$ term depends upon two distinct pieces. The first is what he labels "diagonal magnetic scattering," corresponding to successive $M1$ photon transitions via an intermediate nucleon ground

state. The second he discusses within the context of "relativistic invariance," and rests upon the fact that matrix elements of the charge operator have relativistic contributions from the nucleon magnetic moment. From the continuity equation, these matrix elements in turn affect the transverse current matrix elements. The first of these terms is naturally included in a nonrelativistic calculation, but the second is not. We therefore restrict ourselves to verifying that our calculations reproduce the diagonal magnetic term only. For nucleons, the $O(\omega)$ contribution to the Compton amplitude makes a very small contribution to the cross section compared to the Thomson limit and the polarizability terms. However, it is not known at this time how large the relativistic corrections may be to the polarizabilities themselves. In a relativistic framework, no new amplitude structures enter at $O(\omega^2)$ [32], but there can be additional contributions to α and β.

While a pure harmonic-oscillator model can reproduce the Thomson limit with a sum saturated by the lowest lying P state, the Isgur-Karl model does not have that property. Since the Isgur-Karl states correspond to linear combinations of pure harmonic-oscillator states, one must at least include all states with admixtures of the harmonic-oscillator ground and P-wave states in calculating the low-energy limit. A more serious problem, however, comes from the fact that some effects of the anharmonic potential are included only perturbatively in the energy, and not in the wave function. This has the effect of modifying the energy denominators in the expressions for the Compton amplitude, but not modifying the corresponding current matrix elements. In general, the Thomson limit will then be lost. Alternatively, one could view the Isgur-Karl states as true eigenstates of the Hamiltonian, if the latter is viewed as a set of projection operators. In that case, the expression for the Compton amplitude is correct, but the implied Hamiltonian is then non-local, and the continuity equation can only be satisfied by introducing two-body currents. The extent of the violation is discussed below with other numerical results.

F. polarizabilities

In a pure nonrelativistic framework, the electric polarizability for Compton scattering is [32]

$$\bar{\alpha} = \alpha + \Delta\alpha, \tag{39}$$

where

$$\alpha = 2\sum_n \frac{|\langle N|D_z|X_n\rangle|^2}{E_n - E_0}; \quad \Delta\alpha = \tfrac{1}{3}\frac{(Ze)^2}{M}\langle r^2\rangle, \tag{40}$$

D_z is the electric dipole operator, and Z is the charge of the nucleon. The term $\Delta\alpha$ appears only in Compton scattering and not in treatments of composites in static electric fields; it arises as a form factor effect in the contribution from the quark contact Hamiltonian at non-zero momentum transfer.

The magnetic polarizability is

$$\bar{\beta} = \beta + \Delta\beta, \tag{41}$$

where

$$\beta = 2\sum_n \frac{|\langle N|M_z|X_n\rangle|^2}{E_n - E_0}; \quad \Delta\beta = -\tfrac{1}{2}\frac{Ze^2}{M}\langle r^2\rangle + \tfrac{1}{6}\frac{\langle \mathbf{D}^2\rangle}{M}. \tag{42}$$

In typical baryon models, β has a large contribution from the $\Delta(1232)$ intermediate state, but tends to be cancelled by the negative term in $\Delta\beta$, leaving a small result for $\bar{\beta}$.

The polarizabilities $\bar{\alpha}$ and $\bar{\beta}$ are related to $\tilde{\alpha}$ and $\tilde{\beta}$ in Eq. 37, respectively, as follows:

$$\bar{\alpha} = \alpha_{\rm QED}\tilde{\alpha}; \qquad \bar{\beta} = \alpha_{\rm QED}\tilde{\beta}. \tag{43}$$

Note that $\tilde{\alpha}$ and $\tilde{\beta}$ are not only dimensionless, but they also do not depend upon the use of Heaviside *vs.* Gaussian units, in contrast to their barred counterparts.

In our calculations, rather than compute $\tilde{\alpha}$ and $\tilde{\beta}$ from the above formulas, we extract them directly from the Compton amplitude itself. Making use of the formula 37, we compute an amplitude in which intermediate nucleon states are *omitted*. This eliminates the $O(\omega^2)$ contributions in Eq. 37 which are separate from α and β. We then subtract the $O(1)$ and $O(\omega)$ limits, which are calculated separately. The remaining expressions in the forward and backward photons directions are proportional to $\tilde{\alpha}+\tilde{\beta}$ and $\tilde{\alpha}-\tilde{\beta}$, respectively.

G. cross section and polarization observables

At photon energies above those appropriate to the polarizabilities, we report our results in terms of various observables in the center-of-momentum frame. In principle, all information about the Compton amplitude is contained in a set of six invariant complex functions. We use the parameterization of Ritus [36]:

$$\begin{aligned} T = {} & A_1\epsilon'\cdot\epsilon + A_2 \mathrm{s}'\cdot\mathrm{s} + iA_3\sigma\cdot(\epsilon'\times\epsilon) + iA_4\sigma\cdot(\mathrm{s}'\times\mathrm{s}) \\ & + iA_5\left[(\sigma\cdot\hat{\mathbf{k}})(\mathrm{s}'\cdot\epsilon) - (\sigma\cdot\hat{\mathbf{k}}')(\mathrm{s}\cdot\epsilon')\right] \\ & + iA_6\left[(\sigma\cdot\hat{\mathbf{k}}')(\mathrm{s}'\cdot\epsilon) - (\sigma\cdot\hat{\mathbf{k}})(\mathrm{s}\cdot\epsilon')\right], \end{aligned} \tag{44}$$

where $\mathrm{s} = \hat{\mathbf{k}}\times\epsilon$ and $\mathrm{s}' = \hat{\mathbf{k}}'\times\epsilon'$. All observables can in principle be written in terms of bilinear combinations of the invariants A_i.

With our set of normalization conventions, the differential cross section in the center-of-momentum frame is

$$\frac{d\sigma}{d\Omega} = \alpha^2_{\rm QED}|T|^2. \tag{45}$$

The amplitude T is defined in Eq. 7 for photon polarizations with respect to a common quantization axis. It is more convenient to use photon quantization directions along their respective momenta. In Eq. 45 we therefore use

$${}_\perp\langle N\tfrac{1}{2};\mathbf{k}'\lambda'|T|N\tfrac{1}{2};\mathbf{k}\lambda\rangle_\perp = \sum_{\bar{\lambda}'} D^{\frac{1}{2}\dagger}_{\lambda'\bar{\lambda}'}(\theta_{CM})\,\langle N\tfrac{1}{2};\mathbf{k}'\bar{\lambda}'|T|N\tfrac{1}{2};\mathbf{k}\lambda\rangle, \tag{46}$$

where $D^{\frac{1}{2}}_{\bar{\lambda}'\lambda'}(\theta_{CM})$ is a rotation matrix and θ_{CM} is the center-of-momentum scattering angle.

We have also studied the nucleon polarization asymmetry $A_y(\theta_{CM}, E_\gamma)$, defined by

$$A_y = \frac{N_{+y} - N_{-y}}{N_{+y} + N_{-y}}. \tag{47}$$

Here $N_{\pm y}$ is the number of final photons (or nucleons) that scatter into a detector at θ_{CM} with the initial nucleon polarized along $\pm y$, where $+y$ is in the direction of $\mathbf{k}\times\mathbf{k}'$. Both photon polarizations and the final nucleon polarization are summed. Similarly, one can define a photon polarization asymmetry P_γ as

$$P_\gamma = \frac{N_{+1} - N_{-1}}{N_{+1} + N_{-1}}, \tag{48}$$

where $N_{\pm 1}$ is the number of particles scattering into a detector at center-of-mass angle θ_{CM} with an initial photon helicity of ± 1, and the nucleon and final photon polarizations are summed.

H. model options

In the following we describe the types of wavefunction sets that we have used as intermediate states in our calculation, and the associated spectra used to calculate energy denominators. In order to study the low-energy limit of our calculation, it is useful to define a basis set for which we have exact current continuity. This is simply the set of unmixed states in Table I, with a pure harmonic-oscillator spectrum. Both ground states are degenerate and are given

an energy of $3m_q$; the P-wave states are also degenerate and have an energy of $3m_q + \omega_{\rm HO}$, and the $N = 2$ band states all have a mass of $3m_q + 2\omega_{\rm HO}$. Here m_q, $\omega_{\rm HO}$ and the size parameter $\alpha_{\rm HO}$ in the harmonic-oscillator wavefunctions must be related by $\omega_{\rm HO} = \alpha_{\rm HO}^2/m_q$; we use $\alpha_{\rm HO} = 0.41$ GeV and $m_q = 0.336$ GeV (the values favored by Koniuk and Isgur [25] in their fit to the photon amplitudes) which yields $\omega_{\rm HO} = 0.500$ GeV. The resulting spectrum places the ground states at 1008 MeV, the P-wave states at 1508 MeV and the positive parity excited states at 2008 MeV, which compare roughly with the band centers in the Isgur-Karl model which are at 1085 MeV, 1610 MeV and 1810 MeV.

Our full calculation then uses wavefunctions mixed by the hyperfine interaction and physical masses (taken from the Particle Data Group (PDG) [37] where possible) for the states. Those states in the model which couple weakly to πN and so are unseen in the partial wave analyses (so called 'missing' states) are assigned the Isgur-Karl model prediction for their masses. For this set of states we have also calculated with hadronic widths, which are allowed to enter the calculation in the energy denominators, by the replacement of the energy E_X of the intermediate resonance with $E_X - i\Gamma_X/2$. For the known states, the widths are taken from the PDG; the missing states are assigned widths typical of states in their energy range. The resulting spectrum and the corresponding widths are listed in Table II. In order to study the effects of the mixing between harmonic oscillator substates induced by the hyperfine interaction on the Compton scattering process we also use the unmixed wavefunctions with physical masses and widths as above. Although it might be more consistent to use the masses which result from the Isgur-Karl model before hyperfine mixing (shown in Table I), this is problematic because of degeneracy of the nucleon and $\Delta(1232)$ masses.

III. NUMERICAL RESULTS

A. low-energy limit

As discussed above, the low-energy limit of the Compton scattering amplitude is completely determined, through $O(\omega)$, by Low's theorem [1]. It thus serves as a consistency check of a given model which, through various approximations and truncations, may not necessarily satisfy the theorem.

As noted earlier, a nucleon composed of three valence quarks in a pure harmonic-oscillator well will yield the correct Thomson limit, provided the terms corresponding to the contact interactions with the quarks and the excitation of the lowest-lying P-wave states are included. In units of e^2/M, the contact term contributes a factor $+3$ and the direct and crossed P-wave terms each contribute -1, giving the overall Thomson coefficient of $+1$.

When the full quark Hamiltonian is turned on, the low-energy limit of the Compton amplitude becomes $0.8e^2/M$, in contrast to the expected coefficient of unity. While all baryon excitations through the $N = 2$ band are included, the problem does not stem from a truncated space, because our result has apparently converged. The most likely source of disagreement is the lack of current conservation associated with the mismatch between baryon state vectors and the Hamiltonian. As noted earlier, a local nonrelativistic Hamiltonian with no charge-changing interaction will yield state vectors whose current matrix elements will be conserved with one-body operators only. The Isgur-Karl Hamiltonian satisfies this criterion, but some of its contributions to the state vectors are only evaluated perturbatively. Thus, continuity is no longer guaranteed. The Thomson limit should be restored with a consistent set of state vectors. We have also investigated the issue of current at higher energies, as discussed below.

For the $O(\omega)$ contribution to low-energy Compton scattering, Low's theorem contains two distinct contributions: "diagonal magnetic scattering," corresponding to successive $M1$ photon transitions via an intermediate nucleon ground state, and a second term arising from "relativistic invariance." The first contribution alone is proportional to the square of the nucleon magnetic moment. For both the pure harmonic-oscillator model and the Isgur-Karl model, our results agree with this first term in the sense that the magnetic moment is that predicted by the quark model. The second contribution arises from the interplay between the charge and current operators under Lorentz boosts; when combined with the first contribution, the $O(\omega)$ term is proportional to the square of the *anomalous* magnetic moment. While our baryon current matrix elements have the correct transformation properties between the excited baryon rest frame and any other frame, the fact that a covariant operator was not used to compute the matrix elements in the first place means that the calculation is not fully consistent relativistically, and this fact is manifested in the failure to obtain the correct $O(\omega)$ term in Low's theorem.

B. polarizabilities

At $O(\omega^2)$ in the low-energy expansion, the electric and magnetic polarizabilities $\tilde{\alpha}$ and $\tilde{\beta}$ enter as structure-dependent coefficients. We discuss $\tilde{\alpha}$ and $\tilde{\beta}$ in turn for the proton and then the neutron.

The most recently measured values of the proton polarizabilities, obtained at the University of Illinois microtron [38], are $\tilde{\alpha}_p = (16.1 \pm 3.2 \pm 1.9)$, and $\tilde{\beta}_p = (4.9 \mp 3.2 \mp 1.9)$. Typically, $\tilde{\beta}_p$ is close to or consistent with zero.

As noted above in Eq. 40, $\tilde{\alpha}$ has two distinct contributions, one coming from a form factor effect from the quark contact terms, and the other coming from excitations of the P-wave baryons. In the Isgur-Karl model, the proton *rms* charge radius is 0.375 fm. This yields a contribution $\Delta\alpha = M^2\langle r^2\rangle/3 = 1.06$ to the electric polarizability.

The numerical results are given in Table III. For the pure harmonic-oscillator model, $\tilde{\alpha}_p$ is in qualitative agreement with the experimental value. For the Isgur-Karl model, however, $\tilde{\alpha}$ is considerably lower. This disagreement has three primary sources. The first is that the contact form-factor term is proportional to the mean square charge radius, which is already known to be too low in the Isgur-Karl model. The second is that the energy denominators for coupling to the P waves are larger than in the harmonic-oscillator case, and therefore decrease the contribution to $\tilde{\alpha}$. The third is that there is considerable variation among the individual P-wave contributions. In both the harmonic-oscillator and Isgur-Karl models, for example, the states corresponding to the $N^*\frac{3}{2}^-(1520)$ and the $\Delta^*\frac{3}{2}^-(1700)$ give disproportionally large contributions to the overall amplitude.

The theoretical calculation of $\tilde{\beta}$ involves a cancellation between $\Delta(1232)$ excitation and recoil contributions from the P-wave baryons. A result close to zero therefore implies a sensitivity to the ingredients of both these contributions. In the Isgur-Karl model, we would expect the $\Delta(1232)$ contribution to be lower than it should be, given the fact that the $\gamma N\Delta(1232)$ coupling is too low by a factor of 0.6, and this coupling is squared when computing Compton amplitudes. The fact that our result for $\tilde{\beta}$ is considerably higher than zero again implies, as was the case for $\tilde{\alpha}$, that the coupling to P-wave states is decreased significantly by larger energy denominators.

It is possible to improve the agreement with $\tilde{\alpha}$ and $\tilde{\beta}$ by replacing the P-wave energy denominators with some (smaller) average value, and this step has been sometimes been taken in the literature, but this simply sidesteps the main physics goal of obtaining a consistent spectrum with consistent photon couplings.

The most recently measured values of the neutron polarizabilities, obtained at Oak Ridge National Laboratory [39], are $\tilde{\alpha}_n = (18.2 \pm 2.4 \pm 3.0)$, and $\tilde{\beta}_n = (4.6 \mp 2.4 \mp 3.0)$. The results are given in Table III. Once again, the harmonic-oscillator result is much closer to experiment than that of the Isgur-Karl model. No results for $\tilde{\beta}$ are shown for the harmonic-oscillator model because the $\Delta(1232)$ is degenerate with the nucleon, and would yield a completely unphysical energy denominator.

C. higher energies

Our goal at higher energies, where the composite physics of the nucleon must play a role, has been to investigate which observables are particularly sensitive to the inclusion of various intermediate resonances. We have also searched for signatures in Compton scattering which could be used to establish the presence of resonances unseen in the πN partial wave analyses. In particular, since Compton scattering has two $\gamma N \to X$ interaction vertices, it is much more sensitive than pion production experiments to those states whose coupling to πN is weak and whose coupling to γN is not. By the same reasoning, it is more sensitive than pion photoproduction ($\gamma N \to N\pi$).

Our results therefore hinge on the reliability of the Koniuk and Isgur calculation of the photo-couplings using the Isgur-Karl model wavefunctions and the non-relativistic transition operator. As explained above we have extended their calculation to include the longitudinal and charge matrix elements, and have calculated (for a given intermediate baryon X_n in the γN center of mass) for all values of the inital nucleon momentum. Note that from Eq. 8, unless $\sqrt{s}$ is equal to the mass of X_n (we are on the pole for that intermediate state) for the direct term, the value of $Q^2 = -q^2 = -[M_n - \omega_{M_N}(-\mathbf{k})]^2 + \mathbf{k}^2$ is *not* zero. The crossed term never reaches this kinematic point. Our amplitudes therefore explore a rather different set of kinematics than the photo-excitation amplitudes which are necessarily at $Q^2 = 0$, and a comparison of the results for these amplitudes with experiment should be made at all Q^2. It is for this reason that we have not altered the results of the calculation of the matrix elements in any way in order to fit the photo-coupling data. Table IV lists the model results for the photo-coupling amplitudes, which have been recalculated here, and the data (taken from the Particle Data Group [37]). The quality of the resulting fit (to rather uncertain data) is typical of composite model calculations of transition amplitudes.

We have calculated the differential cross section $d\sigma/d\Omega$ and the asymmetries A_y and P_γ, both as a function of lab photon energy E_γ at fixed θ_{CM} and for fixed E_γ as a function of θ_{CM}, with the former being more useful for disentangling the contributions of various resonances. Figs. 2, 3, and 4 show our results for these three observables at $\theta_{CM} = 60°$ for our mixed set of states (with the effects of widths included but no continuity constraint imposed). We have plotted four curves: the asymmetry with just the nucleon and $\Delta(1232)$ as intermediate states, with the P-wave states also, with these plus states in the $N = 2$ band that are seen in πN, and finally with all of the intermediate states in Table II. The two bumps in Fig. 3 in the second of the above curves which obviously arise from the P-wave states are the result of a complicated interference, and survive the

addition of the $N = 2$ band states [which include the Roper resonance $N^*(1440)$]. This interference is illustrated in Fig. 5, where we have shown how adding the P-wave states one by one takes the first curve of Fig. 3 into the second one. The states $N^*\frac{3}{2}^-(1700)$ and $N^*\frac{5}{2}^-(1675)$ have a negligible effect on the asymmetry (and so the result of adding them in is lumped in with another state) but all others have sizeable effects on the final result, and the intermediate steps often don't resemble the final curve.

In the difference between the third and the fourth curves in Figs. 2, 3, and 4, the effect of removing the 'missing' states from the spectrum of intermediate states is illustrated; given the sizeable change in the asymmetry A_y such an experiment may be able to confirm the existence of these states predicted by the quark model but not seen in πN. Of course, our results at these higher energies are sensitive to states established in πN that we have left out, and we have not shown that the intermediate sum has converged at these energies. We will return to this point later. It is also important to point out that because of the underestimate of the $\Delta(1232)$ photocouplings we are underestimating the size of the effects at the $\Delta(1232)$ pole.

In Figs. 6, 7, and 8 we have plotted the obervables above (again at $\theta_{CM} = 60°$) calculated using our uncoupled intermediate set, to illustrate the sizeable effects of turning off the wavefunction mixing caused by the hyperfine interaction. This demonstrates that these results are quite sensitive to details of the model used for the wavefunctions of the intermediate states, through the sensitivity of the matrix elements of the electromagnetic current. Simple models which count the resonances, their masses, and photo-couplings do not include the necessary constraints imposed on these current matrix elements by the composite nature of the resonances and the force which binds their constituents together.

The Ritus amplitudes A_i defined above are plotted in Figs. 9 and 10, and again the four curves are with just the nucleon and $\Delta(1232)$ as intermediate states, with these plus P-wave states, with all states seen in πN up to $N = 2$, and with all the states in Table II. Although the A_i are themselves not directly observable, we nevertheless thought it useful to illustrate their sensitivity to these groups of intermediate states. It is possible that if an A_i demonstrates a particular sensitivity to some physics (such as the presence or absence of the 'missing' states, as seems to be the case with $\mathrm{Im}(A_1)$ or $\mathrm{Re}(A_3)$, for example) an experiment could be designed that is sensitive to it. Note that A_1 is also the only amplitude which has non-zero real and imaginary parts at zero energy (the tensor it multiplies has the same structure as the Thomson limit, see Eqn. 44) and that its real part at zero energy is reduced by roughly a factor of three (and its imaginary part there becomes non-zero) by the introduction of the P-wave states. Note also that the

imaginary parts of A_1, A_3, A_5, and A_6 vanish when only the nucleon and $\Delta(1232)$ are allowed as intermediate states. The imaginary parts of these amplitudes are therefore *only* sensitive to the resonances in the P-wave band and beyond, and these results are independent of the size of the $\Delta(1232)$ effects.

The effects on $d\sigma/d\Omega$ of imposing continuity on our current matrix elements is illustrated in Fig. 11, for 50 MeV and 300 MeV lab photon energy. We have calculated with an intermediate set which includes up to the P waves for simplicity, and have compared the results without a continuity constraint to those where the longitudinal current matrix element is constrained to be a multiple of the charge matrix element, and *vice-versa*. Although the 300 MeV plot shows only small changes, at 50 MeV there is an unphysical asymmetry about 90° and rapid fall-off near 0° when the longitudinal matrix element is constrained. Fixing the charge matrix element by continuity seems to reduce the size of $d\sigma/d\Omega$ without affecting its angular behaviour significantly. Either of these procedures will adversely affect our low-energy limit, so we have chosen not to impose a continuity constraint. We also conclude that the violation of the continuity requirement is less serious at higher energies.

Compton scattering data exist in the energy region of interest mainly in the form of differential cross sections measured at various angles and energies. We have calculated the angular dependence of $d\sigma/d\Omega$ at sample photon lab energies of 320 MeV and 800 MeV in order to make a comparison with the data of the Bonn [14–16] and Tokyo [17–20] groups. The first energy is close to the $\Delta(1232)$ pole and the second is in the P-wave resonance region. The data from Ref. [14] at 320 MeV and our calculation for intermediate sets made up of the nucleon and $\Delta(1232)$, these plus P waves, and all of the states up to N=2 are plotted in Fig. 12. The curve with just the nucleon and $\Delta(1232)$ shows the expected problem with normalisation due to the non-relativistic quark model's underestimate of the $\Delta(1232)$ couplings at the pole (see Table IV; our estimate of the direct term in the Compton *amplitude* at the $\Delta(1232)$ pole is too small by a factor of about 1/3). The other curves demonstrate that a minor cancellation in the amplitudes, expected from the P-wave states at the $\Delta(1232)$ pole, becomes a large effect when the Delta amplitude is underestimated by this factor.

Examination of the model predictions in Table IV for the P-wave states give us confidence that, while serious, this disagreement should not persist at higher energies where the $\Delta(1232)$ contribution is less important. Indeed, the situation is better at 800 MeV, as illustrated in Fig. 13 where we have plotted data from Ref. [15] and Refs. [17–19] and our calculation for the same three intermediate state sets. Here the data show an asymmetry around 90° which is enhanced in our calculation when the N=2 band (positive parity excited) states are included

in the set of intermediate states, and the normalisation of our calculation relative to the data is roughly correct. In Figs. 14 and 15 we have also plotted A_y and P_γ at this energy (for which no data exist).

One question which remains unanswered is the degree to which our results have converged at the energies examined here. In order to be certain that the effects of higher energy intermediate states are negligible, we need to be able to evaluate the contributions of the next band of states in the harmonic oscillator, the $N = 3$ band. At this level, the harmonic oscillator plus corrections picture of the baryon spectrum is less likely to be reliable as there are now states whose wavefunctions will sample the potential in its (expected from QCD) linear region, where anharmonic perturbations will become very large. For that reason it is understandable that there exist negative parity excited states in the data which lie within the energy range of the $N = 2$ band, the most reliable of which [37] are the $\Delta^*(1900)$, with $J^P = \frac{1}{2}^-$, and $\Delta^*(1930)$, with $J^P = \frac{5}{2}^-$. From counting arguments within the NRQM these states cannot be $N = 1$ band states, but lie far from the center of a postulated $N = 3$ band at around 2500 MeV. It may be that more sophisticated models [26] can incorporate such states; in the model with which we are most familiar [27], where these wavefunctions are expanded in a harmonic-oscillator basis up to $N = 7$, the lowest Δ states with these quantum numbers are at 2035 and 2155 MeV respectively [40]. This is consistent with the roughly 100 MeV overestimation of the mass of the Roper resonance in this model, and the situation for these states is probably somewhat similar; there may be mixtures of the $N = 3$ band states which have particularly low energy.

In order to investigate the effects of these states on the Compton scattering amplitude at $\sqrt{s} = 1900 - 2000$ MeV (corresponding to lab photon energies of roughly 1450 to 1650 MeV), we would therefore need to find the wavefunctions of the lowest energy states in the $N = 3$ band in the Isgur-Karl model, which would necessitate a complete spectral analysis. The simpler option of evaluating the effects of these states with an unmixed harmonic-oscillator model for the wavefunctions (and energies) is, from the above discussion, unlikely to lead to a greater understanding of the issue of convergence. We would simply see effects near the (degenerate) band center of mass and not elsewhere. This issue may only be dealt with within a more sophisticated model for the states and their electromagnetic couplings which encompasses the $N = 3$ band states. The result is that our calculations at these energies is missing the effects of two states clearly seen in πN. Our calculation of the polarization asymmetry A_y for the spectrum with and without the ten unseen states shown in Fig. 3 is therefore missing their contributions in *both* cases. We conclude that the difference of the curves at these energies, rather than details of their shape, may survive inclusion of the $N = 3$ band.

IV. CONCLUSIONS

We have presented a systematic study of nucleon Compton scattering within the framework of the Isgur-Karl-Koniuk model. Our results include calculations of low-energy quantities such as the electric and magnetic polarizabilities as well as differential cross section and polarization observables at intermediate energies.

We wish to emphasize that Compton scattering is not simply a summary of baryon photo-couplings. For some observables, notably the proton asymmetry A_y, there is considerable interference among the individual resonance contributions which would not be exposed by studying individual baryon photo-decay amplitudes. In particular, Compton scattering appears to be quite sensitive to the spectrum of P states.

We therefore urge experimenters to consider a variety of measurements of nucleon Compton scattering, including cross sections and, where possible, polarization observables, to provide more precise constraints on quark models of baryons.

Overall, the behavior of existing data is qualitatively reproduced by the model. Noticeable points of disagreement, such as the failure to reproduce the Thomson limit and the very low cross section in the $\Delta(1232)$ region, can be understood in terms of specific shortcomings of the model, such as the violation of current continuity at low energies, and the small $\gamma N\Delta$ coupling constant implied by the Isgur-Karl-Koniuk model, respectively. Certainly improvements in these aspects of the model will also improve its ability to describe Compton scattering in detail.

There is also much work to be done on the theoretical side. Extension of the Hilbert space beyond the $N = 2$ band is an obvious candidate. We are presently investigating the applicability of the relativized quark model [27], with a basis which extends up to $N = 7$. This may improve both the agreement of the size of the photo-couplings with data and the degree to which the continuity relation is satisfied. There is also the effect of relativistic dynamics. Incorporating relativistic dynamics, which includes both one- and two-photon operators as well as multi-quark current matrix elements, into a model which also fits the baryon spectrum and satisfies the continuity relation, is a major project. Different approaches can handle different parts of such a project easily, and other parts not so easily. The relativized quark model represents one way to do this. We are also considering models which do not rely on v/c expansions. Another physics issue is whether to include explicit meson [or $(q\bar{q})$] intermediate states. As mentioned above, there is some evidence that there may substantial cancellation among the

intermediate ($q\bar{q}$) contributions [21]. However, the pion may represent a special case. In the chiral quark model [6], it is pions rather than quarks that provide the bulk of the nucleon polarizability. In chiral perturbation theory, of course, *all* of the polarizability comes from pions [8]. On the other hand, at higher energies, pions may play a role not unlike other mesons, in which case a valence quark model may be more appropriate. This topic is presently under investigation.

V. ACKNOWLEDGEMENTS

This work was supported in part by the National Science Foundation under Grant PHY-8818836, and the U.S. Department of Energy under Contract No. DE-AC02-76ER03066 and Contract No. DE-AC05-84ER40150. We wish to thank Professors A. M. Nathan and N. C. Mukhopadhyay for helpful discussions, and the Institute for Nuclear Theory at the University of Washington for its hospitality (and the Department of Energy for partial support) during the completion of this work.

REFERENCES

* Current address.

[1] F. E. Low, *Phys. Rev.* **96**, 1428 (1954).

[2] M. Gell-Mann and M. L. Goldberger, *Phys. Rev.* **96**, 1433 (1954).

[3] P. C. Hecking and G. F. Bertsch, *Phys. Lett.* **99B**, 237 (1981).

[4] A. Schäfer, B. Müller, D. Vasak and W. Greiner, *Phys. Lett.* **143B**, 323 (1984).

[5] G. Dattoli and G. Matone, *Nuo. Cim.* **19**, 601 (1977).

[6] R. Weiner and W. Weise, *Phys. Lett.* **159B**, 85 (1985); N. Scoccola and W. Weise, *Nucl. Phys.* **A517**, 495 (1990).

[7] E. M. Nyman, *Phys. Lett.* **142B**, 388 (1984); M. Chemtob, *Nucl. Phys.* **A473**, 613 (1987).

[8] V. Bernard, N. Kaiser, and U.-G. Meissner, *Phys. Rev. Lett.* **67**, 1515 (1991).

[9] A. I. L'vov, *Yad. Fiz.* **34**, 1075 (1981) [*Sov. J. Nucl. Phys.* **34**, 597 (1981)].

[10] V. A. Petrun'kin, *Proceedings of the Lebedev Physics Institute*, **41** (1968).

[11] V. A. Petrun'kin, *Fiz. Elem. Chastits At. Yadra* **12**, 692 (1981) [*Sov. J. Part. Nucl.* **12**, 278 (1981)].

[12] See W. Pfeil, H. Rollnik, and S. Stankowksi, *Nucl. Phys.* **B73**, 166 (1974), and references therein; G. Kölbel, Bonn University preprint BONN-IR-78-16, (1978) (Ph.D. thesis).

[13] G. Busschhorn *et al.*, *Phys. Lett.* **B37**, 207 (1971).

[14] H. Genzel, M. Jung, R. Wedemeyer, and H.J. Weyer, *Z. Phys.* **A279**, 399 (1976).

[15] M. Jung, J. Kattein, H. Kück, P. Leu, K.-D. de Marné, R. Wedemeyer, and N. Wermes, *Z. Phys.* **C10**, 197 (1981).

[16] J. Duda, F.-W. Höfner, M. Jung, R. Kleissler, H. Kück, P. Leu, K.-D. de Marné, B. Munk, W. Vogl, and R. Wedemeyer, *Z. Phys.* **C17**, 319 (1983).

[17] K. Tashioka *et al.*, *Nucl. Phys.* **B141**, 364 (1978).

[18] T. Ishii, K. Egawa, S. Kato, T. Miyachi, K. Sugano, K. Toshioka, K. Ukai, M. Chiba, K. Joh, T. Shinohara, Y. Yoribayashi, and Y. Wada, *Nucl. Phys.* **B165**, 189 (1980).

[19] Y. Wada, K. Egawa, A. Imanishi, T. Ishii, S. Kato, K. Ukai, F. Naito, H. Nara, T. Noguchi, and K. Takahashi, *Nucl. Phys.* **B247**, 313 (1984).

[20] T. Ishii, K. Egawa, A. Imanishi, S. Kato, Y. Takeuchi, K. Ukai, M. Yoshioka, T. Noguchi, T. Ohmori, N. Shimura K. Takahashi, and Y. Wada, *Nucl. Phys.* **B254**, 458 (1985).

[21] P. Geiger and N. Isgur, *Phys. Rev.* **D41**, 1595 (1990); *Phys. Rev.* **D44**, 799 (1991).

[22] N. Isgur and G. Karl, *Phys. Lett.* **72B**, 109 (1977); **74B** (78) 353; *Phys. Rev.* **D18**, 4187 (1978).

[23] N. Isgur and G. Karl, *Phys. Rev.* **D19**, 2653 (1979).

[24] N. Isgur, G. Karl and R. Koniuk, *Phys. Rev. Lett.* **41**, 1269 (1978); *Phys. Rev.* **D25**, 2394 (1982).

[25] R. Koniuk and N. Isgur, *Phys. Rev.* **D21**, 1868 (1980).

[26] D.P. Stanley and D. Robson, *Phys. Rev. Lett.* **45**, 235 (1980); C.P. Forsyth and R.E. Cutkosky, *Phys. Rev. Lett.* **46**, 576 (1981); *Z. Phys.* **C18**, 219 (1983); J. Carlson, J. Kogut and V. R. Pandharipande, *Phys. Rev.* **D27**, 233 (1983); **D28**, 2809 (1983); R. Sartor and Fl. Stancu, *Phys. Rev.* **D31**, 128 (1985); **D33**, 727 (1986).

[27] S. Capstick and N. Isgur, *Phys. Rev.* **D34**, 2809 (1986).

[28] S. Capstick and G. Karl, *Phys. Rev.* **D41**, 2767 (1990).

[29] F.E. Close and Zhenping Li, *Phys. Rev.* **D42**, 2194 (1990);**D42**, 2207 (1990).

[30] M. Warns, H. Schröder, W.P. Pfeil, and H. Rollnik, *Z. Phys.* **C45**, 613 (1990); **C45**, 627 (1990).

[31] B. D. Keister and W. N. Polyzou, *Adv. Nucl. Phys.* **20**, 225 (1991).

[32] V. A. Petrun'kin, *J. Exp. Theor. Phys.* **40**, 1148 (1961) [*Sov. Phys. JETP* **13**, 808 (1961)].

[33] J. L. Friar, *Ann. Phys.* **95**, 170 (1975).

[34] S. J. Brodsky and J. R. Primack, *Ann. Phys.* **52**, 315 (1969).

[35] T. E. O. Ericson and J. Hüfner, *Nucl. Phys.* **B57**, 604 (1973).

[36] V. I. Ritus, *J. Exp. Theor. Phys.* **33**, 1264 (1957) [*Sov. Phys. JETP* **6**, 972 (1958)].

[37] J.J. Hernández *et al.*, *Phys. Lett.* **B239**, 1 (1990).

[38] F.J. Federspiel, R.A. Eisenstein, M.A. Lucas, B.E. MacGibbon, K. Mellendorf, A.M. Nathan, A. O'Neill and D.P. Wells, *Phys. Rev. Lett.* **67**, 1511 (1991).

[39] J. Schmiedmayer, P. Riehs, J. A. Harvey and N. W. Hill, *Phys. Rev. Lett.* **66**, 1015 (1991).

[40] Table IV in Ref. [27] gives the correct prediction of the model for the lowest mass $\Delta^* \frac{5}{2}^-$ state. The discussion in the text uses an erroneous value from a previous fit. One of us (S.C.) would like to thank Fl. Stancu and P. Stassart for bringing this to our attention.

TABLES

TABLE I. Harmonic oscillator substates of the N and Δ up to the $N = 2$ band. The notation $(J_1, J_2, ...)$ is a shorthand for states identical except for their total $\mathbf{J} = \mathbf{L} + \mathbf{S}$. Energies are the model predictions before application of the hyperfine interaction.

N	SU(6) multiplet	Energy (MeV)	states		
0	$[56, 0^+]$	1085	$\|N^2 S_S \frac{1}{2}^+\rangle$	$\|\Delta^4 S_S \frac{3}{2}^+\rangle$	
1	$[70, 1^-]$	1610	$\|N^2 P_M(\frac{1}{2}, \frac{3}{2})^-\rangle$	$\|N^4 P_M(\frac{1}{2}, \frac{3}{2}, \frac{5}{2})^-\rangle$	$\|\Delta^2 P_M(\frac{1}{2}, \frac{3}{2})^-\rangle$
2	$[56', 0^+]$	1600	$\|N^2 S_{S'} \frac{1}{2}^+\rangle$	$\|\Delta^4 S_{S'} \frac{3}{2}^+\rangle$	
	$[70, 0^+]$	1810	$\|N^2 S_M \frac{1}{2}^+\rangle$	$\|N^4 S_M \frac{3}{2}^+\rangle$	$\|\Delta^2 S_M \frac{1}{2}^+\rangle$
	$[56, 2^+]$	1850	$\|N^2 D_S(\frac{3}{2}, \frac{5}{2})^+\rangle$	$\|\Delta^4 D_S(\frac{1}{2}, \frac{3}{2}, \frac{5}{2}, \frac{7}{2})^+\rangle$	
	$[70, 2^+]$	1935	$\|N^2 D_M(\frac{3}{2}, \frac{5}{2})^+\rangle$	$\|N^4 D_M(\frac{1}{2}, \frac{3}{2}, \frac{5}{2}, \frac{7}{2})^+\rangle$	$\|\Delta^2 D_M(\frac{3}{2}, \frac{5}{2})^+\rangle$
	$[20, 1^+]$	2020	$\|N^2 P_A(\frac{1}{2}, \frac{3}{2})^+\rangle$		

TABLE II. Spectrum of states corresponding to the coupled wavefunctions, from the Particle Data Group [37]. States labelled † are 'missing' states; they are given model masses and widths estimated from those of nearby states with similar quantum numbers. The first Δ^* with $J^P = \frac{3}{2}^+$ (experimentally $\Delta^*(1600)$) is assigned its model mass for consistency.

State type (I, J^P)	Mass (MeV)	Width (MeV)	Mass (MeV)	Width (MeV)	Mass (MeV)	Width (MeV)
$N\frac{1}{2}^+$	938	0				
$\Delta\frac{3}{2}^+$	1232	115				
$N^*\frac{1}{2}^-$	1535	150	1650	150		
$\Delta^*\frac{1}{2}^-$	1620	140				
$N^*\frac{3}{2}^-$	1520	125	1700	100		
$\Delta\frac{3}{2}^-$	1700	250				
$N^*\frac{5}{2}^-$	1675	155				
$N^*\frac{1}{2}^+$	1440	200	1710	110	1900†	85
	2060†	85				
$\Delta^*\frac{1}{2}^+$	1875†	150	1910	220		
$N^*\frac{3}{2}^+$	1720	200	1870†	170	1955†	170
	1975†	170	2055†	170		
$\Delta^*\frac{3}{2}^+$	1800	250	1920	250	1985†	200
$N^*\frac{5}{2}^+$	1680	125	1955†	100	2000	140
$\Delta^*\frac{5}{2}^+$	1905	300	1975†	270		
$N^*\frac{7}{2}^+$	1990	330				
$\Delta^*\frac{7}{2}^+$	1950	240				

TABLE III. Static limits and polarizabilities for two quark models described in text. Values of $\tilde{\beta}$ for the harmonic-oscillator model are not shown because they contain no $\Delta(1232)$ contribution.

parameter	pure HO	Isgur-Karl	expt.
T_{0p} (e^2/M)	1.0	0.8	1.0
T_{0n} (e^2/M)	0.0	0.1	0.0
$\tilde{\alpha}_p$	13.3	3.8	$16.1 \pm 3.2 \pm 1.9$
$\tilde{\beta}_p$	—	3.7	$4.9 \mp 3.2 \mp 1.9$
$\tilde{\alpha}_n$	11.1	2.8	$18.2 \pm 2.4 \pm 3.0$
$\tilde{\beta}_n$	—	4.4	$4.6 \mp 2.4 \mp 3.0$

TABLE IV. Photo-excitation amplitudes (in units of 10^{-3} GeV$^{\frac{1}{2}}$) for states for which data exists (taken from the PDG [37]) calculated in the center of mass. Proton (p) and neutron (n) amplitudes are always equal for Δ states. Signs of the amplitudes are not relevant here but can be defined relative to πN and are shown to be generally in agreement with the data in Refs. [25, 29].

State, J^P	$A^p_{\frac{1}{2}}$	expt.	$A^n_{\frac{1}{2}}$	expt.	$A^p_{\frac{3}{2}}$	expt.	$A^n_{\frac{3}{2}}$	expt.
$\Delta(1232)\frac{3}{2}^+$	85	141±5			149	258±19		
$N(1535)\frac{1}{2}^-$	143	73±14	123	76±32				
$N(1650)\frac{1}{2}^-$	91	48±16	55	17±37				
$\Delta(1620)\frac{1}{2}^-$	97	19±16						
$N(1520)\frac{3}{2}^-$	6	22±10	44	65±13	137	167±10	135	144±14
$N(1700)\frac{3}{2}^-$	1	22±12	14	0±56	30	0±19	71	2±44
$\Delta(1700)\frac{3}{2}^-$	119	116±17			134	77±28		
$N(1675)\frac{5}{2}^-$	7	19±12	31	47±23	10	19±12	43	69±19
$N(1440)\frac{1}{2}^+$	18	69±7	10	37±19				
$N(1710)\frac{1}{2}^+$	58	5±16	42	5±23				
$\Delta(1910)\frac{1}{2}^+$	23	12±30						
$N(1720)\frac{3}{2}^+$	117	52±39	45	2±26	40	35±24	8	43±94
$\Delta(1600)\frac{3}{2}^+$	49	22±29			110	1±22		
$\Delta(1920)\frac{3}{2}^+$	50	43±?			36	23±?		
$N(1680)\frac{5}{2}^+$	10	17±10	9	31±13	84	127±10	23	30±14
$\Delta(1905)\frac{5}{2}^+$	5	27±13			11	47±19		
$N(1990)\frac{7}{2}^+$	7	24±30	7	49±45	9	31±55	8	122±55
$\Delta(1950)\frac{7}{2}^+$	19	73±14			23	90±13		

FIGURES

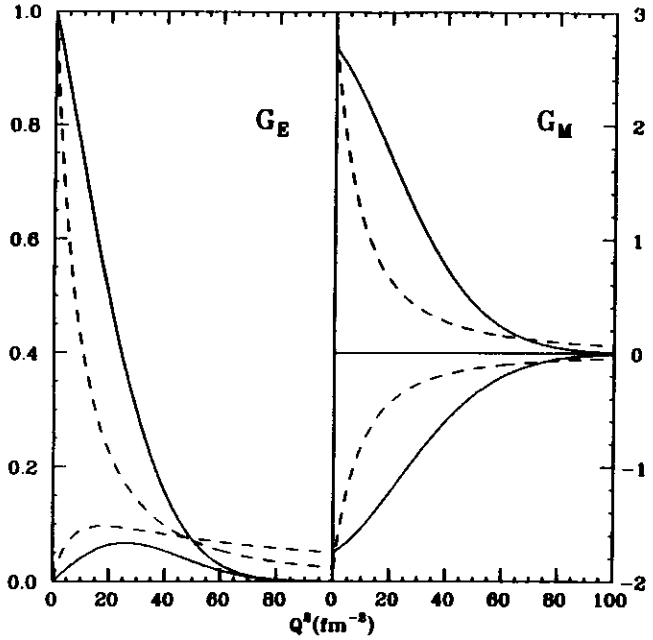

FIG. 1. G_E and G_M for the proton (upper solid lines) and the neutron (lower solid lines). The dashed lines are a modified dipole representation of the data.

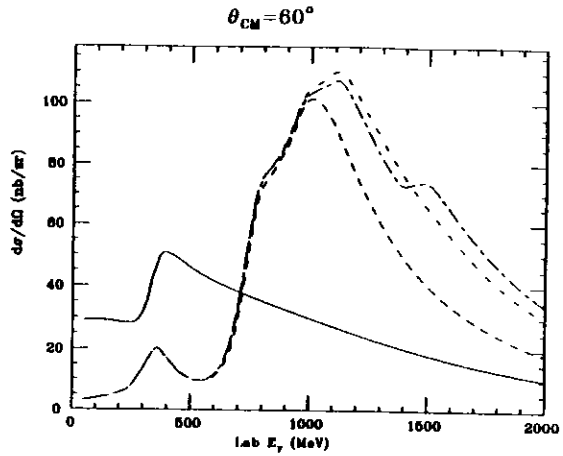

FIG. 2. Differential cross section for Compton scattering at $\theta_{CM} = 60°$ with intermediate states consisting of the nucleon and $\Delta(1232)$ (solid line), these plus the P waves (dashed line), all states up to N=2 seen in πN (dot-dashed line), and with all states from Table II (short/long dashed line).

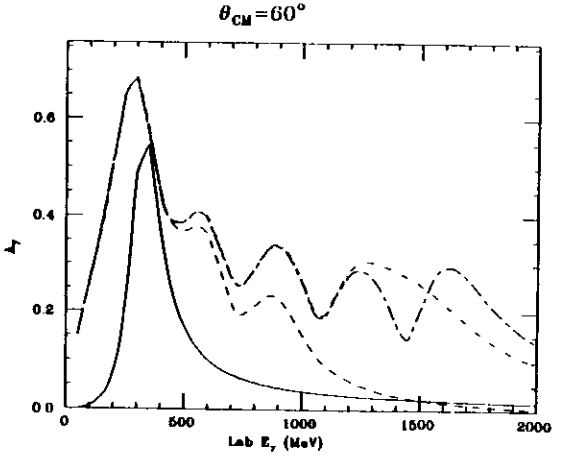

FIG. 3. Initial nucleon polarization asymmetry A_y at $\theta_{CM} = 60°$; legend as in Fig. 2.

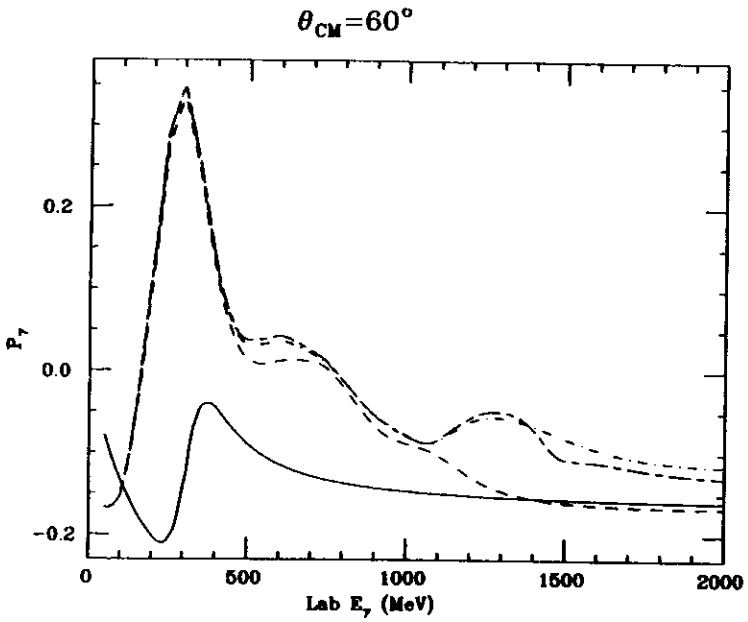

FIG. 4. Initial photon polarization asymmetry P_γ at $\theta_{CM} = 60°$; legend as in Fig. 2.

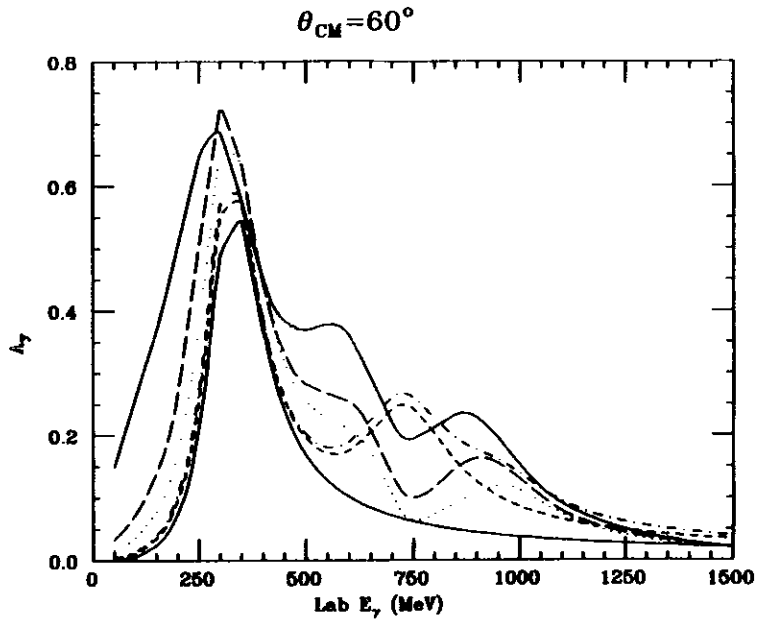

FIG. 5. Initial nucleon polarization asymmetry A_y at $\theta_{CM} = 60°$. Intermediate state sets are the nucleon and $\Delta(1232)$ (lower solid line), plus $N^*\frac{1}{2}^-(1535)$ (short-dashed line), plus $N^*\frac{1}{2}^-(1650)$ (dot-dashed line), plus $N^*\frac{3}{2}^-(1520)$ (dotted line), plus $N^*\frac{3}{2}^-(1700)$, $N^*\frac{5}{2}^-(1675)$, and $\Delta^*\frac{1}{2}^-(1620)$ (long-dashed line), plus $\Delta^*\frac{3}{2}^-(1700)$ (*i.e.* N + Δ + all P waves) (upper solid line).

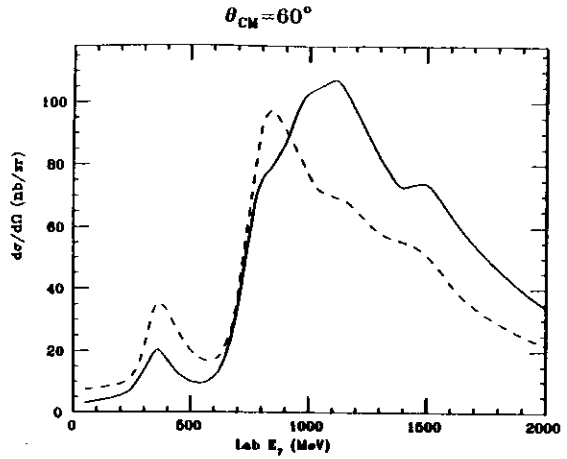

FIG. 6. Differential cross section at θ_{CM} = 60° with all states in Table II intermediate. The solid line is with mixed wavefunctions, the dashed line with unmixed.

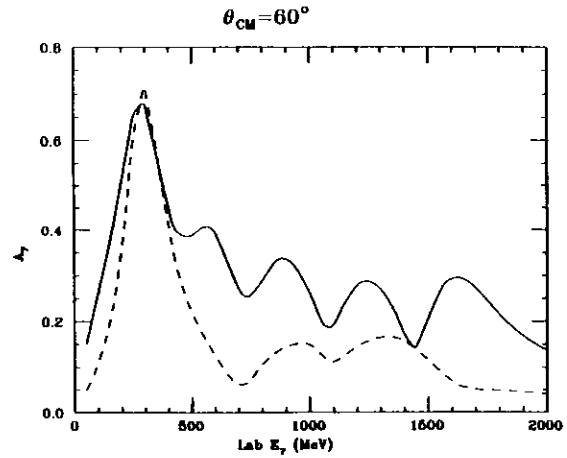

FIG. 7. Initial nucleon polarization asymmetry A_y at θ_{CM} = 60°; legend as in Fig. 6.

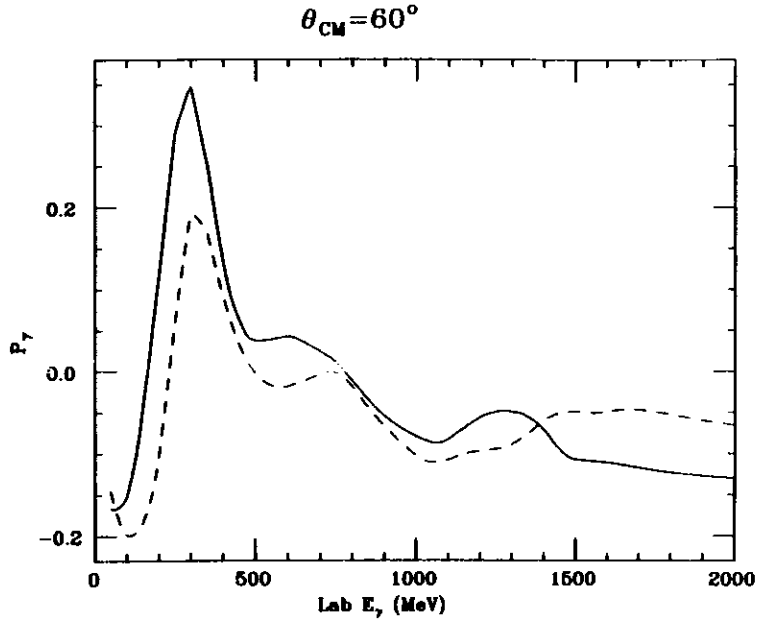

FIG. 8. Initial photon polarization asymmetry P_γ at θ_{CM} = 60°; legend as in Fig. 6.

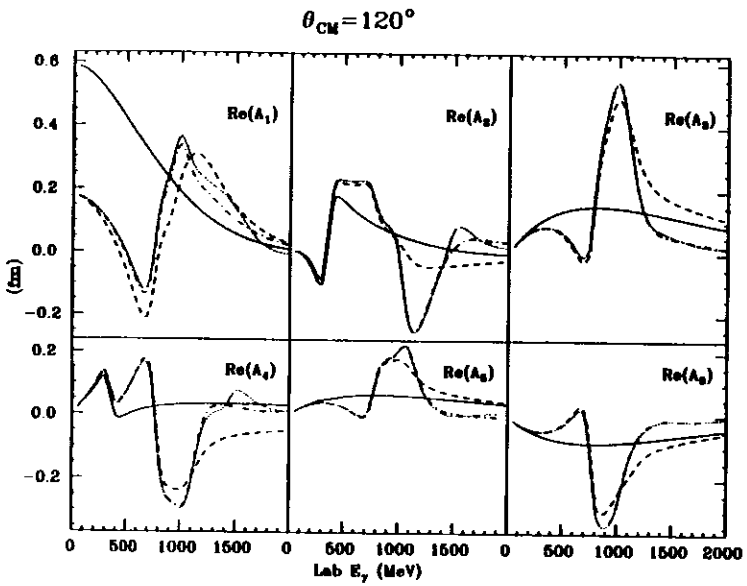

FIG. 9. Real parts of the Ritus amplitudes A_i at $\theta_{CM} = 120°$ with intermediate states consisting of the nucleon and $\Delta(1232)$ (solid line), these plus the P waves (dashed line), all states up to N=2 seen in πN (dot-dashed line), and with all states from Table II (dotted line).

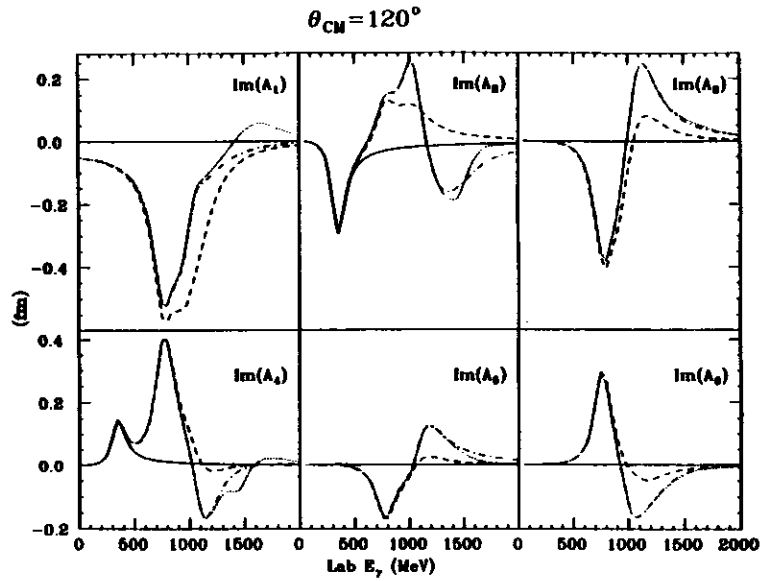

FIG. 10. Imaginary parts of the Ritus amplitudes A_i at $\theta_{CM} = 120°$; legend as in Fig. 9.

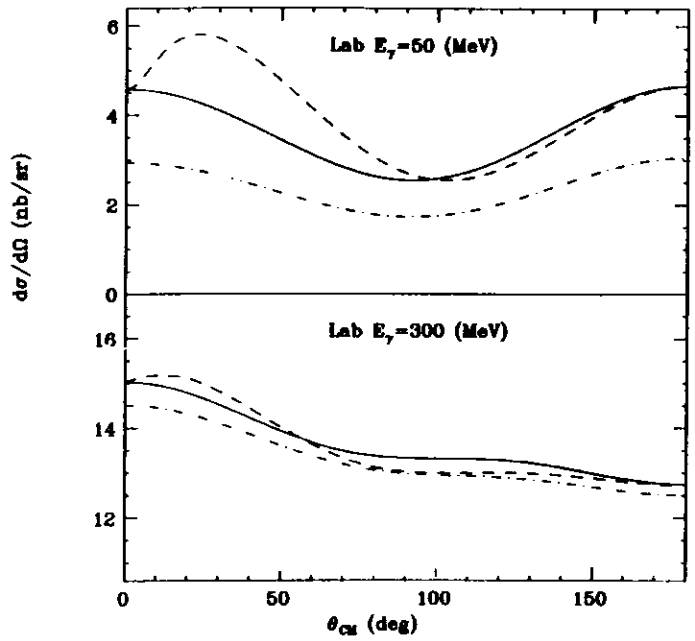

FIG. 11. The effect of current constraints on the differential cross section at lab E_γ = 50 MeV and 300 MeV for nucleon, $\Delta(1232)$ and P-wave states as intermediates. The solid line is without any continuity constraint imposed, the dashed line has the longitudinal matrix element constrained, the dot dashed line has the charge matrix element constrained.

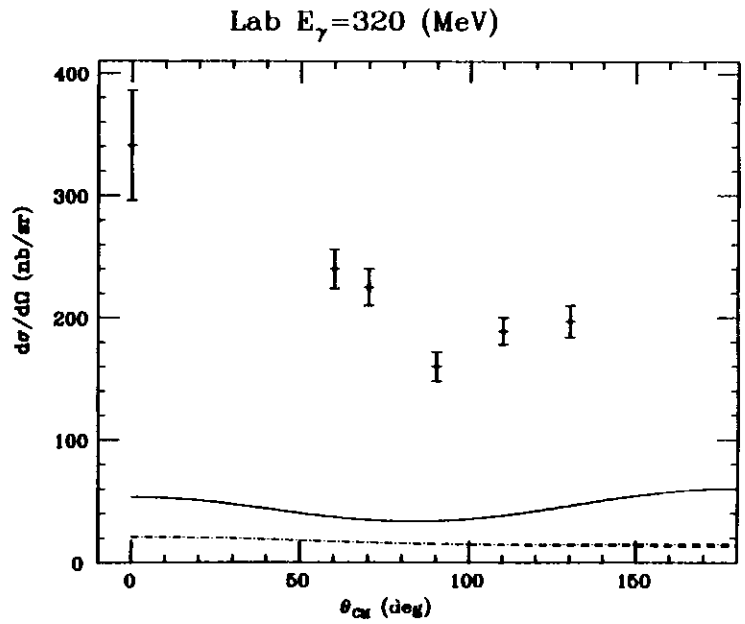

FIG. 12. Differential cross section at lab E_γ = 320 MeV [near the $\Delta(1232)$ pole] with intermediate states consisting of the nucleon and $\Delta(1232)$ (solid line), these plus the P waves (dashed line), and with all states from Table II (dot-dashed line). Data are from Ref. [14].

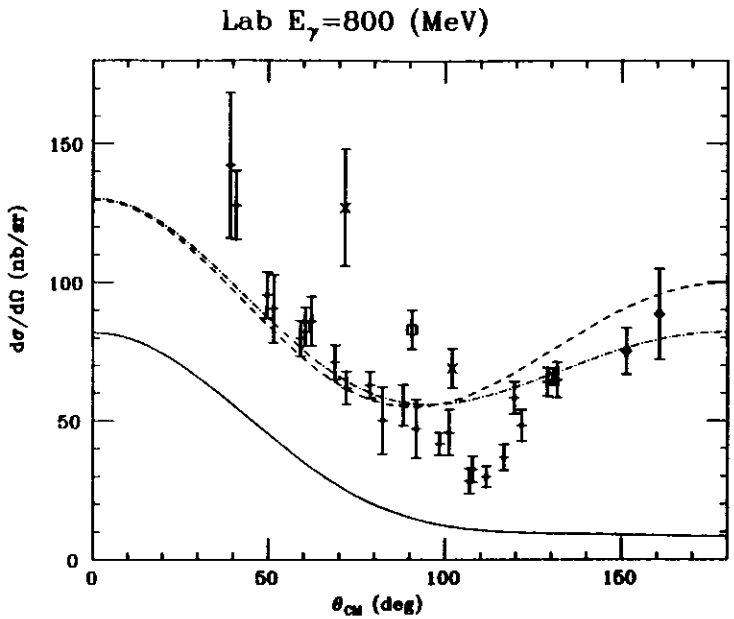

FIG. 13. Differential cross section at lab E_γ = 800 MeV (in the P-wave region). Legend as in Fig. 12. Data are from Ref. [15] (crosses), Ref. [17] (boxes), Ref. [18] (X's), and Ref. [19] (diamonds).

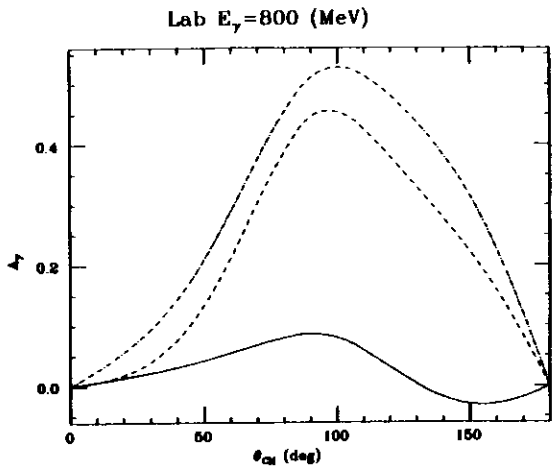

FIG. 14. A_y at lab E_γ = 800 MeV. Legend as in Fig. 13.

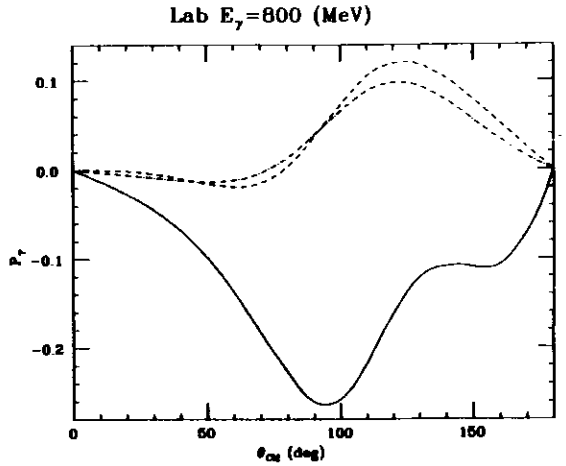

FIG. 15. P_γ at lab E_γ = 800 MeV. Legend as in Fig. 13.